AD-A034 977 STANFORD RESEARCH INST MENLO PARK CALIF F/G 9/5
MIC 7-TO-11-GHZ FREQUENCY DISCRIMINATOR.(U)
SEP 76 U H GYSEL, J P WATJEN N00039-75-C-0404
UNCLASSIFIED NL

1 OF 2
AD A034977

5730

B.S.

Final Report

MIC 7-TO-11-GHz FREQUENCY DISCRIMINATOR

By: U. H. GYSEL J. P. WATJEN

Prepared for:

DEPARTMENT OF THE NAVY
NAVAL ELECTRONICS SYSTEMS COMMAND
CRYSTAL CITY PLAZA
WASHINGTON, D.C. 20360

CONTRACT N00039-75-C-0404

STANFORD RESEARCH INSTITUTE
Menlo Park, California 94025 · U.S.A.

STANFORD RESEARCH INSTITUTE
Menlo Park, California 94025 · U.S.A.

Final Report *September 1976*

MIC 7-TO-11-GHz FREQUENCY DISCRIMINATOR

By: U. H. GYSEL J. P. WATJEN

Prepared for:

DEPARTMENT OF THE NAVY
NAVAL ELECTRONICS SYSTEMS COMMAND
CRYSTAL CITY PLAZA
WASHINGTON, D.C. 20360

CONTRACT N00039-75-C-0404

SRI Project 4237

Approved by:

DAVID A. JOHNSON, *Director*
Radio Physics Laboratory

RAY L. LEADABRAND, *Executive Director*
Electronics and Radio Sciences Division

Copy No. 16

UNCLASSIFIED

SECURITY CLASSIFICATION OF THIS PAGE (When Data Entered)

REPORT DOCUMENTATION PAGE

READ INSTRUCTIONS BEFORE COMPLETING FORM

1. REPORT NUMBER

2. GOVT ACCESSION NO.

3. RECIPIENT'S CATALOG NUMBER

4. TITLE (and Subtitle)

MIC 7-TO-11-GHz FREQUENCY DISCRIMINATOR

5. TYPE OF REPORT & PERIOD COVERED

Final Report concerning the period 25 March 1975 to 31 July 1976

6. PERFORMING ORG. REPORT NUMBER

SRI Project 4237

7. AUTHOR(s)

Ulrich H. Gysel John P. Watjen

8. CONTRACT OR GRANT NUMBER(s)

Contract N00039-75-C-0404

9. PERFORMING ORGANIZATION NAME AND ADDRESS

Stanford Research Institute
Menlo Park, California 94025

10. PROGRAM ELEMENT, PROJECT, TASK AREA & WORK UNIT NUMBERS

11. CONTROLLING OFFICE NAME AND ADDRESS

Department of the Navy
Naval Electronics Systems Command
Crystal City Plaza
Washington, D.C. 20360

12. REPORT DATE

September 1976

13. NO. OF PAGES

108

14. MONITORING AGENCY NAME & ADDRESS (if diff. from Controlling Office)

15. SECURITY CLASS. (of this report)

UNCLASSIFIED

15a. DECLASSIFICATION/DOWNGRADING SCHEDULE

N/A

16. DISTRIBUTION STATEMENT (of this report)

17. DISTRIBUTION STATEMENT (of the abstract entered in Block 20, if different from report)

18. SUPPLEMENTARY NOTES

19. KEY WORDS (Continue on reverse side if necessary and identify by block number)

Frequency discriminator
MIC frequency discriminator
Line discriminator
Microwave frequency discriminator

20. ABSTRACT (Continue on reverse side if necessary and identify by block number)

A broadband (7 to 11 GHz) frequency discriminator was developed that is highly linear and suitable for either CW or pulse RF input signals. Microwave integrated circuit (MIC) techniques were used in the construction of the discriminator. Microstrip is chosen for the RF circuits to minimize the discriminator's size and, eventually, cost of production. The discriminator is of the conventional line discriminator type and consists of two 3-dB quadrature hybrids, a delay line, and two detectors. The difference between the two detector outputs is the desired →

DD FORM 1 JAN 73 1473

EDITION OF 1 NOV 65 IS OBSOLETE

UNCLASSIFIED

SECURITY CLASSIFICATION OF THIS PAGE (When Data Entered)

19. KEY WORDS (Continued)

20 ABSTRACT (Continued)

output voltage, which is close to a linear function of the incoming signal. Interaction between imperfect subcomponents and higher harmonics that are generated in the detector diodes causes undesirable ripples in the frequency-response characteristic. A computer analysis program was written to determine error sources and to develop subcomponent specifications that must be maintained to obtain a given linearity specification.

The development of high-performance microstrip quadrature hybrids, 3-dB attenuators, terminations, and detectors is described. The detectors include harmonic rejection filters to prevent harmonics from reentering the microwave circuit. Circuit losses that increase with frequency cause a constant curvature in the frequency response of the discriminator. A gain-shaping network in MIC form at the RF input of the discriminator compensates for these frequency-dependent losses and linearizes the frequency response. A wideband dc-coupled differential video amplifier was designed to sum the detector output voltages and to obtain a single video output.

In the absence of a high-accuracy limiter the critical measurements of input frequency versus output voltage were made with an automatic measurement system, which simulated a perfect limiter. This system uses a Hewlett-Packard automatic network analyzer, which was augmented with a computer-controlled powermeter and voltmeter. In the final discriminator model the following results were achieved at an RF input power level of -6 dBm: The output voltage swing from 7 to 11 GHz is 90 to 235 mV. The maximum frequency deviation from a best straight line is ±0.82% of the total frequency range, or ±33 MHz. This compares with a theoretical error of ±13 MHz for a discriminator built with perfect subcomponents. The video amplifier has 20 dB of gain, and the total response time of the discriminator (delay time, rise time, and settling time to 1% accuracy) is 25 ns. The output noise voltage of the discriminator corresponds to a peak frequency uncertainty of ±16 MHz.

CONTENTS

LIST OF ILLUSTRATIONS vii

LIST OF TABLES ix

ACKNOWLEDGMENTS xi

I INTRODUCTION 1

II PRINCIPLE OF OPERATION 5

III DISCRIMINATOR ANALYSIS PROGRAM 13

A. Program Description 13

B. Discriminator Analysis Results 20

IV DISCRIMINATOR PERFORMANCE 31

V COMPONENT DEVELOPMENT 43

A. Quadrature Hybrid 43

1. MIC Quadrature Hybrid Evaluation 43
2. "Wiggly" Coupler Development 45

B. Detectors 49

1. Circuits for Detector and Multiplexer 49
2. Development of Detector and Multiplexer 53

C. Attenuator and Termination 64

1. Attenuator 64
2. Termination 66

D. Shaping Network 67

E. Video Amplifier 73

VI DISCRIMINATOR MEASUREMENT TECHNIQUE 83

A. Background 83

B. Computer-Controlled Measurement System 84

VII CONCLUSIONS AND RECOMMENDATIONS 91

REFERENCES 95

ILLUSTRATIONS

1	Schematic of Frequency Discriminator	6
2	Comparison Between Discriminators Using Square-Law and Envelope Detectors	9
3	Signal-Flow Graph for Frequency Discriminator	14
4	Flowchart for Frequency-Discriminator Analysis Program	19
5	Theoretical Frequency Errors	21
6	Photograph of the Frequency Discriminator MIC Circuit (Model 1)	32
7	Output Voltage and Frequency Error of Discriminator, Model 1	34
8	Photograph of the Frequency-Discriminator MIC Circuit (Model 1a)	35
9	Output Voltage and Frequency Error of Discriminator, Model 1a	36
10	Output Voltage and Frequency Error of Discriminator, Model 1 (SN 3-76-2)	38
11	Photograph of the Frequency-Discriminator MIC Circuit with Shaping Network (Model 2)	39
12	Overall View of the Frequency Discriminator	40
13	Output Voltage and Frequency Error of Linearized Discriminator, Model 2	41
14	Three Possible MIC Quadrature Hybrids	44
15	Measured Characteristics of 3-dB Quadrature Hybrid	48
16	Schematic of Detector Circuit	49
17	Three Detector Circuits with Reactively Terminated Harmonics	52
18	Equivalent Circuit of First Detector	55
19	Theoretical Performance of First Detector	56
20	Photograph of Improved Detector	58

21	Equivalent Circuit of Improved Detector	59
22	Theoretical Performance of Improved Detector	61
23	Output Voltage and Transfer Characteristic of Improved Detector	62
24	3-dB Attenuator Design	65
25	Two Shaping-Network Topologies	68
26	Photograph of Trial Shaping Network	70
27	Theoretical and Experimental Response of Trial Shaping Network	71
28	Approximation of Required Attenuation with Shaping Network	72
29	Simplified Circuit Diagram of the Differential Video Amplifier	77
30	Schematic of Final Differential Video Amplifier	80
31	Pulse Response of Differential Video Amplifier	81
32	Block Diagram of Discriminator Measurement Test Setup	85
33	Flow Diagram of Discriminator Measurement Program	86

TABLES

1 Comparison of Three Different MIC 3-dB Quadrature Hybrids 46

ACKNOWLEDGMENTS

The authors wish to acknowledge the many contributions made by other present or former SRI personnel. Joe Hunt, Engineering Assistant, fabricated and assembled very skillfully the miniature MIC hardware. Bill Weir, Research Engineer, wrote the software for the automatic measurement system. Ashok Gorwara, former Project Supervisor, was instrumental in starting this program and carrying it through many difficult phases. Don Parker, former Program Manager, and William Edson, Assistant Laboratory Director, contributed to the program in various capacities. The authors appreciate their interest and assistance during the course of the project. Finally, the support and confidence of Jerry Koenig, Technical Director, and Joe Kain, Program Manager, both of NAVELEX, and Temple Timberlake, Technical Program Manager, NRL, are gratefully acknowledged.

I INTRODUCTION

Wideband frequency discriminators are used to translate the frequency of an incoming RF signal into a voltage that unambiguously identifies the RF frequency, preferably by a linear relationship. Frequency discriminators generally operate on the principle of converting the frequency variations into amplitude variations, followed by amplitude detection. Thus, a limiter preceding the actual discriminator is necessary to remove any amplitude variations in the incoming RF signal. An important application of frequency discriminators is in frequency memory systems used in modern jamming equipment for deception and range-gate pull-off. The output voltage of the discriminator is used to drive a voltage-controlled oscillator (VCO). When the transfer characteristics of the discriminator and VCO are matched, a frequency is generated that is nearly equal to the originally applied frequency. The output frequency can be held long enough to fulfill the countermeasures requirements by clamping the control voltage with a suitable "hold" circuit. An open-loop frequency-memory unit of this kind will be limited in its set-on accuracy by errors caused by the limiter, the VCO, and most significantly, the discriminator.

Open-loop frequency memory systems do not presently meet the required accuracy of approximately ±2 MHz for modern ECM applications. Hence, open-loop systems have to be augmented by some kind of error-correcting procedure to reduce the error below the ±2 MHz limit. This results in a closed-loop system. The response time of this closed-loop system will be improved as the accuracy of the incorporated open-loop system is increased. Thus, for either type of system configuration a

frequency discriminator with very good linearity and small ripples is an extremely important component.

Previous microwave discriminators of the so-called line-discriminator type have used discrete components or integrated stripline assemblies. Both realizations have a limited accuracy. Our calculations for a typical discriminator for the 7-to-11-GHz frequency range showed that frequency errors as large as ±300 MHz have to be expected. This number corresponds to a discriminator construction that uses commercially available hybrids, attenuators, detectors, and terminations, all interconnected with SMA connectors. Commercially available discriminators in an integrated stripline assembly* show considerably reduced errors of ±120 MHz over the same frequency range. These errors are too large for the frequency-memory application.

The objective of this program was to improve the accuracy of broadband frequency discriminators by an order of magnitude, and to build a small and reliable unit. The goal was to approach as closely as possible the theoretical limit of ±10 MHz for a line discriminator. This formidable task was made more difficult by the low input power level of -6 dBm, from which the discriminator has to operate. A maximum response time of 25 ns was also required. A unit was produced that meets the response-time requirement and shows a maximum frequency error of ±33 MHz.

Key elements for SRI's success were an extensive analysis of errors in frequency discriminators, the use of microwave integrated circuits (MIC), and the control of the strongest harmonic frequencies generated in the detectors of the discriminator. A computer program was written

---

*Lorch Devices, Inc., Englewood, N.J.

to analyze the effects of imperfect subcomponents on the frequency error. This program was extremely useful in helping to set performance specifications for the subcomponents and in understanding measured frequency errors. The RF circuits were fabricated in microstrip to minimize the size of the discriminator, to eliminate unnecessary connector discontinuities, and to obtain reduced costs in production. To avoid undesirable ripples in the frequency-response characteristic, it is essential to provide appropriate terminations for the harmonics generated in the diodes. Therefore, the matching network for the detector diodes was designed to give proper control over the harmonic terminations in addition to matching the diodes in the fundamental frequency band. An operational amplifier sums the output of the two detectors to obtain a single video output.

The operating principle of the discriminator is discussed in Section II of this report, and Section III describes the error-analysis program. The major results of four different frequency discriminators are given in Section IV. Detailed descriptions of the discriminator subcomponents and the measurement techniques used are given in Sections V and VI. The last section contains conclusions and recommendations.

II PRINCIPLE OF OPERATION

Microwave frequency discriminators operate on principles quite similar to those of the familiar Foster-Seeley discriminator widely used in FM receivers at much lower frequencies. The central idea is to produce two RF signal components with a phase shift between them that is proportional to frequency. Vectorial addition of the two components and subsequent detection yields a detected signal that is frequency-dependent. At microwave frequencies it is convenient to achieve the phase shift between the two RF components by means of a difference in line length. In that respect the microwave discriminator is a type of interferometer. A microwave realization is shown in Figure 1. In this circuit the RF input signal is split by a first quadrature hybrid into two equal components with 90° phase shift. One of the two signal components suffers a differential delay $\Delta\tau$ before being recombined with the other signal component in a second quadrature hybrid. It is this double-path propagation that transforms frequency changes into amplitude changes. The latter are detected with diode detectors and properly added and amplified with a video amplifier.

The analysis of the discriminator circuit in Figure 1 is straightforward and well known.[1*] Let us assume for the moment that the input power to the discriminator is P_{in} and that the circuit contains ideal quadrature hybrids. In addition, the circuit, including the two multiplexer and matching networks, is considered to be lossless in the band of interest. (The functions of the multiplexer and matching networks

---

*References are listed at the end of the report.

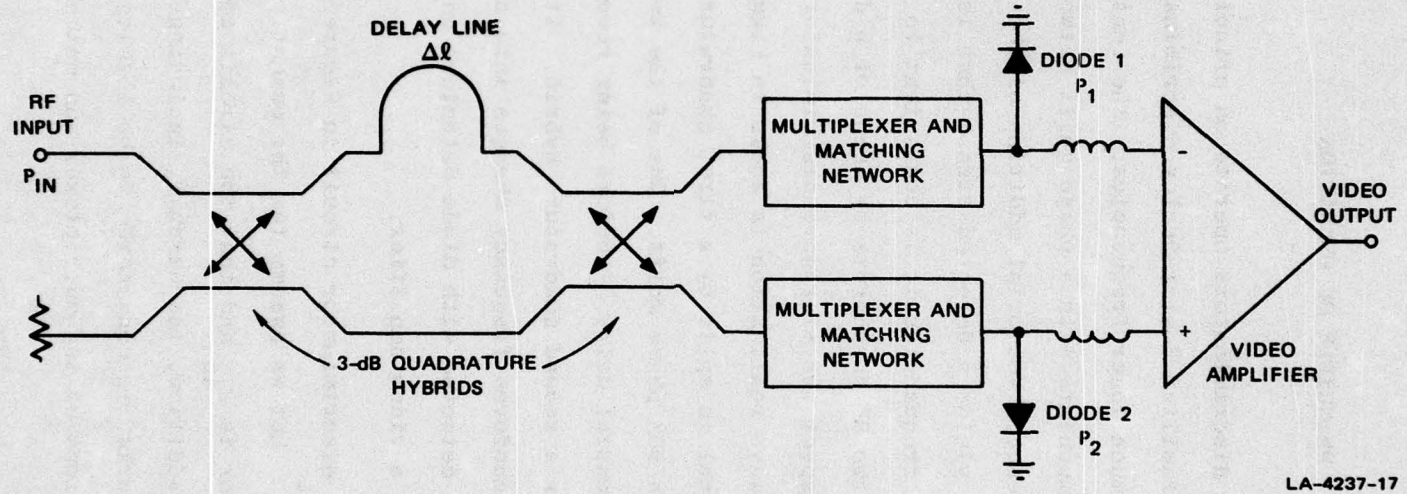

FIGURE 1 SCHEMATIC OF FREQUENCY DISCRIMINATOR

will be explained later.) The power delivered to each detector diode is given by

$$P_1 = \frac{1}{2} P_{in}(1 - \cos\theta)$$

$$P_2 = \frac{1}{2} P_{in}(1 + \cos\theta) \qquad (1)$$

where

$$\theta = 2\pi\Delta\ell/\lambda$$

with

$\Delta\ell$ = Length of the delay line

λ = Guide wavelength of the delay line.

Assuming a nondispersive delay line, θ can be expressed as a linear function of frequency,

$$\theta = \frac{\pi}{2} kf/f_o \qquad (2)$$

where

f_o = Frequency for which the delay line is one-quarter wavelength long

$$k = \frac{\ell}{(\lambda_o/4)} \qquad (3)$$

λ_o = Wavelength at f_o .

The two detectors convert the incident RF power into a video voltage according to the relationship

$$V = \gamma P^{\alpha} \qquad (4)$$

where

γ = Voltage sensitivity of the detector

α = Exponent .

At relatively small input power levels the detectors operate in the square-law region and $\alpha = 1$. For large input signals the detectors operate closer to the linear or envelope mode, for which $\alpha = 0.5$.

The video amplifier subtracts the two detector voltages, yielding an output voltage of the form

$$V_{out} = V_2 - V_1 = \gamma\left(P_2^{\alpha} - P_1^{\alpha}\right) \quad . \tag{5}$$

Substituting Eq. (1) into Eq. (5) yields, for square-law detectors:

$$V_{out} = \gamma_1 P_{in} \cos\theta \tag{6}$$

and for envelope detectors:

$$V_{out} = \gamma_2 \sqrt{2P_{in}} \cos\left[\frac{\theta}{2} + (2n+1)\frac{\pi}{4}\right] \quad , \quad n\pi \le \theta \le (n+1)\pi \quad . \tag{7}$$

Equations (6) and (7) are plotted in Figure 2 for k = 1, because the discriminator exhibits best linearity when the length of the delay line is $\lambda_o/4$ at band center. The amplitudes of the two curves have been adjusted to give identical slopes at $\theta = 90°$. The frequency errors caused by the cosine response of an ideal discriminator of the configuration shown in Figure 1 can be calculated by fitting a best straight line through the applicable cosine curve. For the band from 7 to 11 GHz ($\theta = 70°$ to $110°$, 44% fractional bandwidth) these errors are ±0.5% for square-law detectors and ±0.25% for envelope detectors,

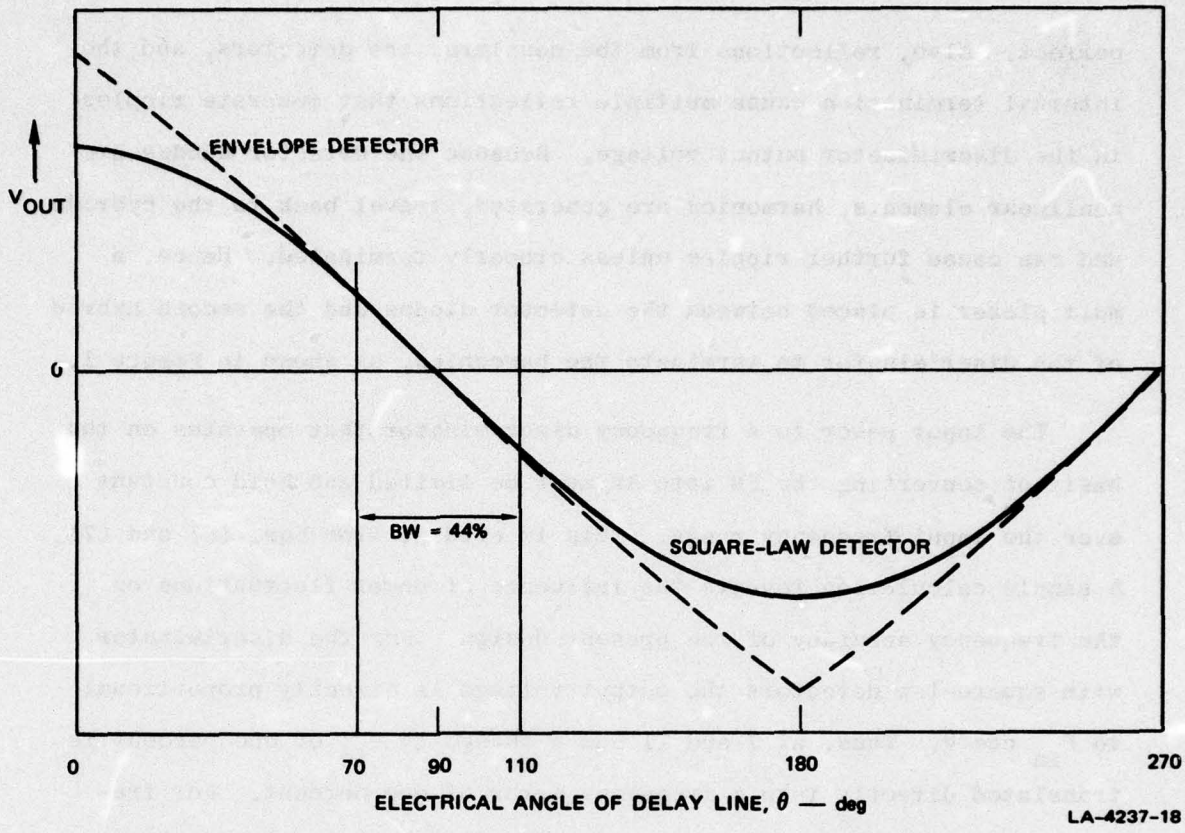

FIGURE 2 COMPARISON BETWEEN DISCRIMINATORS USING SQUARE-LAW AND ENVELOPE DETECTORS (k = 1)

expressed as a percentage of the maximum voltage deviation of the discriminator at the bandedges. If expressed in frequency, these errors are ±10 MHz and ±5 MHz, respectively, for the two cases. This analysis shows the superiority of the discriminator with envelope detectors. Unfortunately, this advantage does not materialize in practice, because other error sources are dominant.

The above calculations are based on the assumption of ideal components in the discriminator. Any practical circuit can only approximate the ideal components. A brief overview of the practical limitations is given in the remainder of this section.

The coupling factor of practical 3-dB quadrature hybrids is frequency-dependent, the isolation is finite, and the port VSWRs are not

perfect. Also, reflections from the couplers, the detectors, and the internal termination cause multiple reflections that generate ripples in the discriminator output voltage. Because the detector diodes are nonlinear elements, harmonics are generated, travel back to the hybrids, and can cause further ripples unless properly terminated. Hence, a multiplexer is placed between the detector diodes and the second hybrid of the discriminator to terminate the harmonics, as shown in Figure 1.

The input power to a frequency discriminator that operates on the basis of converting the FM into AM must be limited and held constant over the input frequency range. This is evident from Eqs. (6) and (7). A simple calculation reveals the influence of power fluctuations on the frequency accuracy of the present design. For the discriminator with square-law detectors the output voltage is directly proportional to $P_{in} \cos \theta$. Thus, at 7 and 11 GHz a change in P_{in} of one percent is translated directly into a frequency error of one percent. For frequencies approaching the center frequency, the error decreases proportionately, when expressed in percent of the total frequency range of the discriminator. At midband the discriminator should be independent of the input power level. In numbers, one obtains a frequency error of 46 MHz at the bandedges for the square-law detector, and 23 MHz for the envelope detector, if the input power varies by 0.1 dB. Just as detrimental as power fluctuations at the input are loss variations in the discriminator circuit itself. Increasing line losses and a decreasing detector sensitivity with increasing frequency cause a uniform curvature in the otherwise smooth output of the discriminator. This effect was very pronounced in the actual circuit and was compensated for by a shaping network at the input of the discriminator.

It will be shown later that electrical symmetry of the circuit is extremely important. In particular, any imbalance of the reflection coefficients of the two detectors can cause strong ripples in the

discriminator response due to interactions with reflections from the first 3-dB coupler and the internal termination. It was an important aspect of this program to understand fully this and other limitations of a realistically achievable discriminator, quantitatively as well as qualitatively. Since purely mathematical analyses were not feasible, the performance of the discriminator was analyzed numerically. Our approach used the scattering parameters of the subcomponents of the discriminator and signal-flow graph techniques. A description of the computer program and the results of the analysis are presented in the next section.

III DISCRIMINATOR ANALYSIS PROGRAM

A. Program Description

Most circuit analysis programs fall into two categories--those based on a nodal analysis, and those based on interconnected two-ports. The first type of computer program usually requires that the circuit to be analyzed be described in terms of an equivalent circuit consisting of lumped and distributed elements. The second type of program is very convenient and efficient, but requires a circuit that can be partitioned into interconnected two-ports. In general, the latter type cannot handle four ports such as 3-dB couplers. Neither program was suitable for analysis of the frequency discriminator, because a program was desired that would accept explicit two- and four-port parameters--preferably scattering parameters--of the subcomponents such as detectors and couplers. No program that met these requirements was available; consequently one was written specifically for the frequency discriminator.

The analysis approach taken is based on a matrix formulation of the signal flow graph[2] using scattering parameters. The signal-flow graph for the discriminator is shown in Figure 3. The S-parameters shown are those of the quadrature couplers. These are derived from the voltage coupling factor at midband, c, the center frequency, f_o, and the complex isolation coefficient, s_{14}. The couplers were assumed to obey the theoretical coupling response of the single-section parallel-coupled line coupler, or

$$s_{12} = \frac{jc \sin \theta}{\sqrt{1 - c^2} \cos \theta + j \sin \theta} \qquad (8a)$$

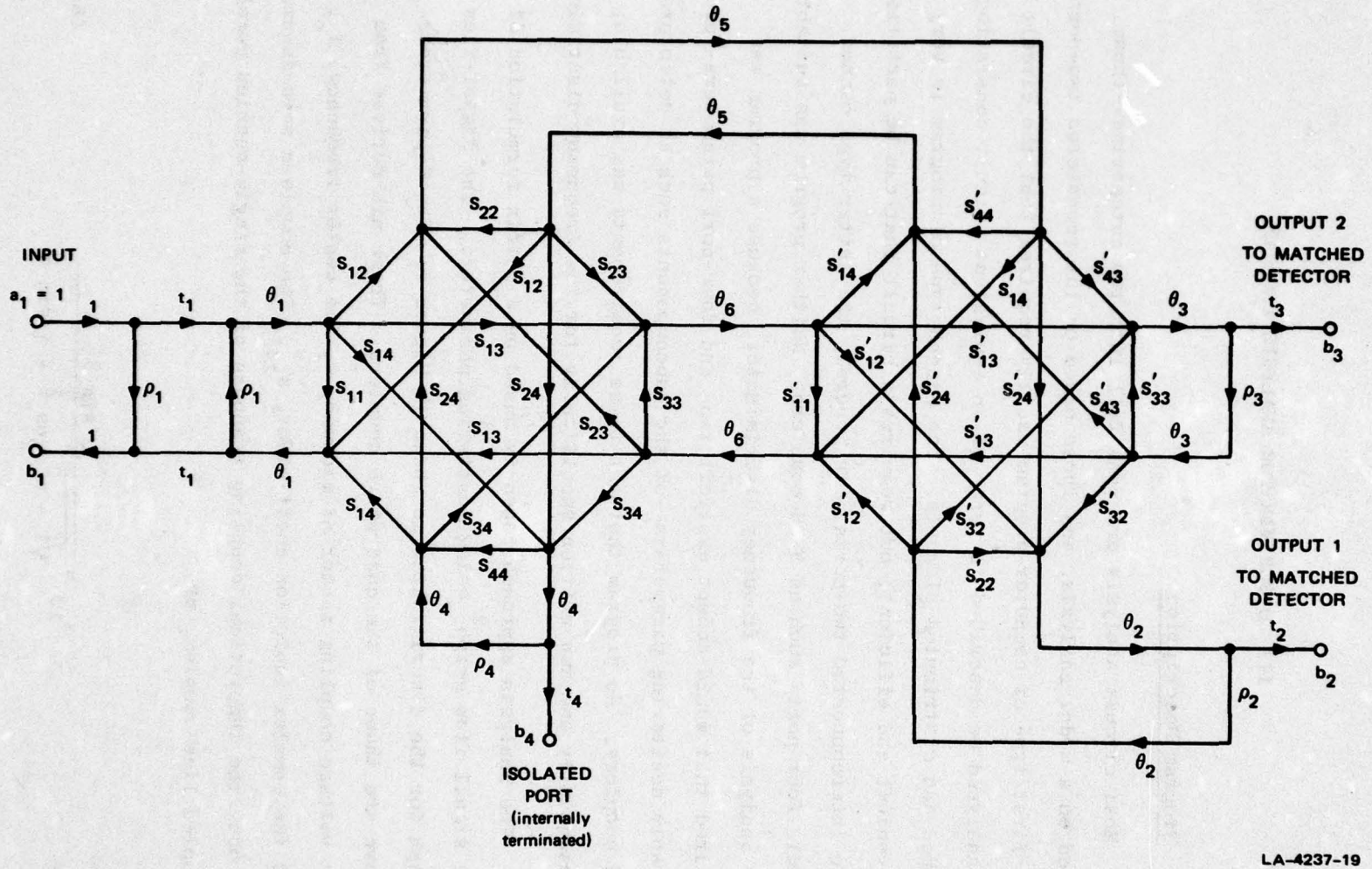

FIGURE 3 SIGNAL-FLOW GRAPH FOR FREQUENCY DISCRIMINATOR

and

$$s_{13} = \frac{\sqrt{1 - c^2}}{\sqrt{1 - c^2}\cos\theta + j \sin\theta} \tag{8b}$$

where $\theta = \frac{\pi}{2}\frac{f}{f_o}$ is the electrical length of the coupler. The isolation of a slightly imperfect hybrid is related to the port reflection coefficients by

$$|s_{ii}| \approx |s_{14}| \quad . \tag{9}$$

The phase relationship between s_{ii} and s_{14} is arbitrary and depends on the nature of the imperfection. Equal phase for the two was assumed because this causes a worst-case phase error, $\Delta\varphi$, in the quadrature phase relationship between s_{11} and s_{13}, of

$$\Delta\varphi \approx 2 \cdot |s_{14}|^2 \quad . \tag{10}$$

The elements denoted by θ_n are arbitrary line lengths with complex propagation constants--i.e., $\theta_n = e^{-\gamma_n' \ell_n}$, where $\gamma_n' = \alpha_n + j\beta_n$, α_n is the attenuation constant, β_n is the phase constant, and ℓ_n is the physical length of the line.

Reflections at the input of the discriminator--e.g., from the microstrip-to-coaxial transition and from the connector--are modeled by a lossless but not perfectly matched two-port. The two-port is characterized by its complex input reflection coefficient, ρ_1. For simplicity, the two-port is assumed to be symmetrical and to have zero electrical length. Hence, the transmission coefficient is related to ρ_1 by

$$|t_1|^2 = 1 - |\rho_1|^2 \qquad (11a)$$

$$\arg(t_1) = \arg(\rho_1) \pm \pi/2 \quad . \qquad (11b)$$

The choice of the sign in Eq. (11b) has no effect on the calculated discriminator linearity and the input VSWR. Hence the plus sign was selected arbitrarily. Imperfect detector and internal load VSWRs are modeled similarly by lossless two-ports connected in front of a perfect termination. ρ_2 and ρ_3 represent the complex reflection coefficient of the two detectors. The power delivered to the junction resistance of each detector is given by $|t_2|^2$ and $|t_3|^2$, where t_2 and t_3 follow equations analogous to Eq. (11a). Finally, ρ_4 represents the complex reflection coefficient of the isolating load connected to the input quadrature coupler.

So that the effect of asymmetries in the two detectors could be studied, the program was designed to simulate different degrees of tracking of the reflection coefficients of the two detectors as a function of frequency. Perfect tracking is obtained by assigning equal reflection coefficients to both detectors. The opposite of perfect tracking is obtained by assigning both detectors reflection coefficients of equal magnitude but opposite phase, or $\rho_3 = -\rho_2$. In practice, neither case is likely to occur. Both detectors are of identical design. Small differences between them are the result of manufacturing and diode tolerances. Therefore, the assumption can be made that the two detectors have reflection coefficients that track each other within a certain tolerance range. This assumption has been experimentally verified. For the purpose of modeling imperfect tracking, ρ_1 and ρ_2 are selected as the vector sum of a constant frequency-independent average value ρ_{av} and a component ρ_R whose magnitude is constant but whose phase

angle varies randomly from detector to detector and from frequency point to frequency point.

Diode detectors have an RF impedance that is RF-power-dependent. This causes a further tracking error in a frequency discriminator, because the power delivered to one detector increases and the power delivered to the other detector decreases with increasing frequency. These power variations translate into impedance variations. The deviations of the detector reflection coefficients from the average value are maximum at the bandedges and are assumed to decrease linearly with frequency toward the band center. Mathematically, this can be expressed as

$$\rho_2 = \rho_{av} + \rho_F(f - f_o)/(f_2 - f_1)$$
$$\rho_3 = \rho_{av} - \rho_F(f - f_o)/(f_2 - f_1) \qquad (12)$$

where

ρ_F = Derivation of the complex reflection coefficient from ρ_{av} at the bandedge

f_2 = Upper bandedge frequency

f_1 = Lower bandedge frequency .

The computer program calculates the wave amplitudes b_1 through b_4 under the assumption of $a_1 = 1$. The power delivered to the two detectors (matched junction resistances) is given by $|b_2|^2$ and $|b_3|^2$. A normalized discriminator output voltage V'_{out} is calculated from Eq. (5) by setting $\gamma = 1$, or

$$V'_{out} = |b_3|^{2\alpha} - w|b_2|^{2\alpha} \quad . \qquad (13)$$

In this formula, w represents a weighting factor added to express differences in the rectification efficiencies of the two detectors. The exponent α of the detectors is also a variable input parameter of the computer program. The input VSWR is obtained from b_1, and the power delivered to the internal load could be determined from b_4.

To minimize the amount of input data required to characterize the discriminator, an initialization subroutine is included. Consequently one need enter only data pertaining to the perturbations from the initialized circuit. The initialized circuit is composed of perfect components connected by lossless lines whose lengths are set to the values anticipated for the actual device. A flowchart for the computer program is shown in Figure 4.

The output from the program consists of the output voltage and input VSWR of the discriminator, both as a function of frequency. The frequency error versus frequency was determined by fitting in a Chebychev sense a straight line through the curve of output voltage. The parameters of this best straight-line approximation were also determined by the computer program and were expressed in terms of the discriminator's sensitivity (volts/MHz, normalized) and the discriminator's center frequency (frequency of zero output voltage, MHz).

For the purpose of ensuring that the numerical model was a meaningful description of practical discriminators, measured characteristics of some of the individual subcomponents were used for the calculations. For instance, values for the isolation of the quadrature coupler and for the tracking of the detector diodes were derived from measurements. A major discrepancy between the model and the actual circuit arises from the fact that the actual frequency dependence was neglected for most imperfections such as finite isolations and VSWRs and was assumed to be constant over the frequency of interest. These simplifications lead to

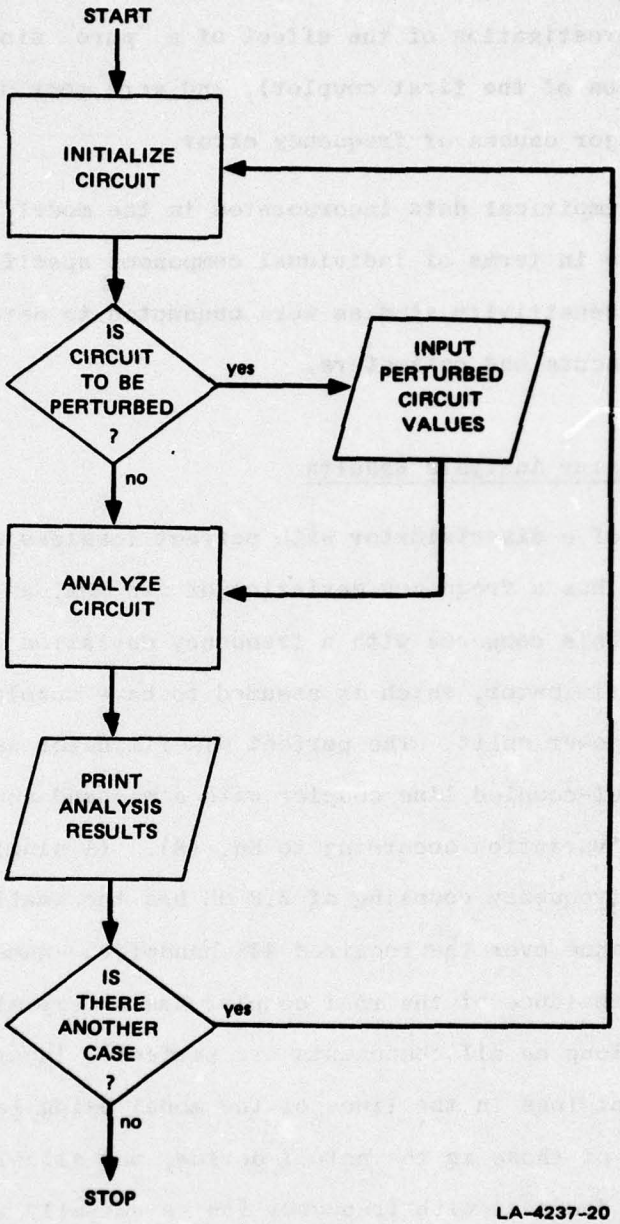

FIGURE 4 FLOWCHART FOR FREQUENCY-DISCRIMINATOR ANALYSIS PROGRAM

an overestimation of the frequency errors, if constant worst-case values are assumed for all components. On the other hand, these simplifications allowed the investigation of the effect of a "pure" single imperfection (e.g., isolation of the first coupler), and were most helpful in identifying major causes of frequency error.

With the empirical data incorporated in the model, practical performance limits in terms of individual component specifications were generated and sensitivity studies were conducted to determine the critical components and parameters.

B. Discriminator Analysis Results

The case of a discriminator with perfect lossless components was run first. It has a frequency deviation of ±13 MHz, as shown in Figure 5(a). This compares with a frequency deviation of ±10 MHz for the ideal discriminator, which is assumed to have couplers providing a constant 3-dB power split. The perfect discriminator assumes only a perfect parallel-coupled line coupler with a midband coupling of 2.8 dB and a coupling variation according to Eq. (8). (A single-section coupler with a center frequency coupling of 2.8 dB has the smallest possible coupling imbalance over the required 44% bandwidth--namely ±0.2 dB.) The coupling imbalance of the real coupler has a very minor effect on linearity, as long as all components are perfect. Incorporating frequency-dependent loss in the lines of the model using lengths that are representative of those in the actual device, and allowing the detector sensitivity to decrease with frequency (as is actually the case), one obtains a response as shown in Figure 5(b). This effect was discussed in Section II, and the computer analysis only verifies the above findings.

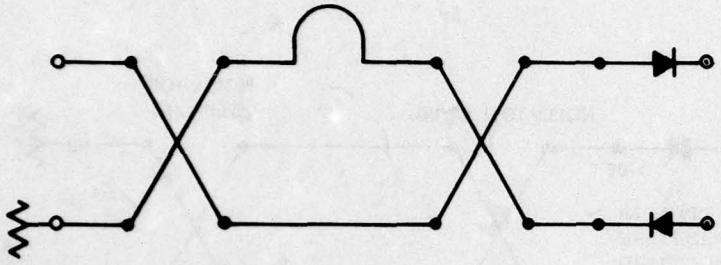

PERFECT, LOSSLESS ELEMENTS

(a)

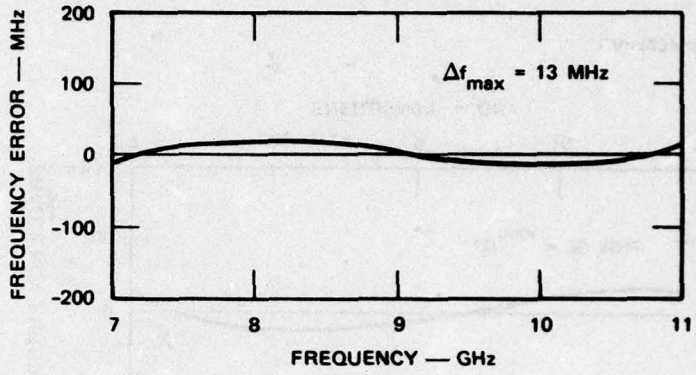

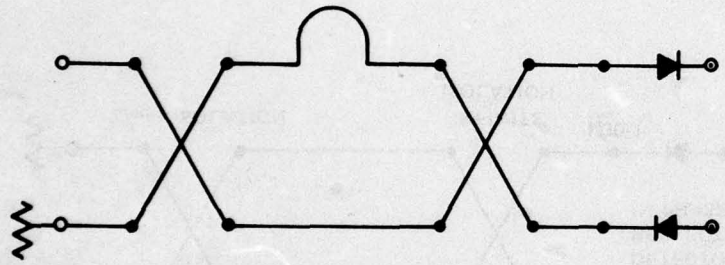

ALL ELEMENTS PERFECT, EXCEPT
ALL TRANSMISSION LINES HAVE
FREQUENCY-DEPENDENT LOSS

(b)

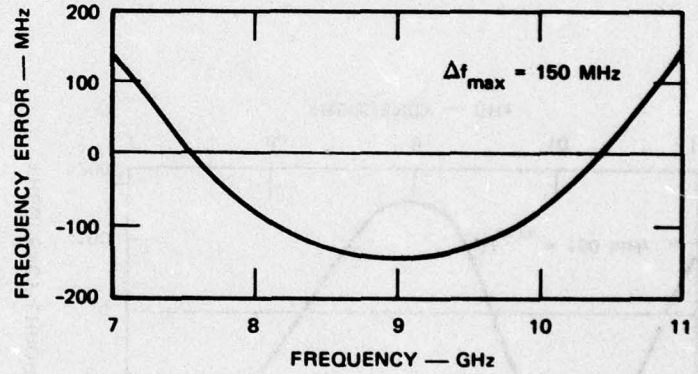

LA-4237-21

FIGURE 5 THEORETICAL FREQUENCY ERRORS

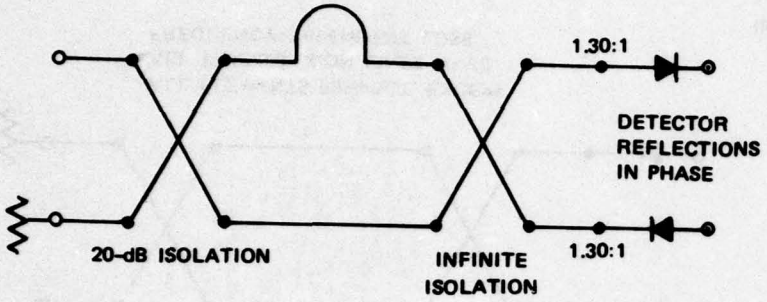

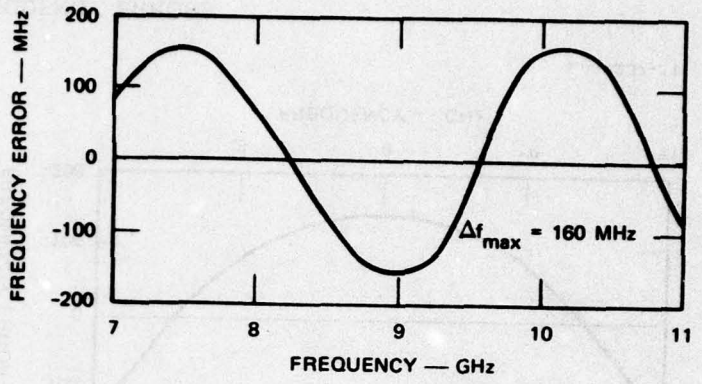

(c)

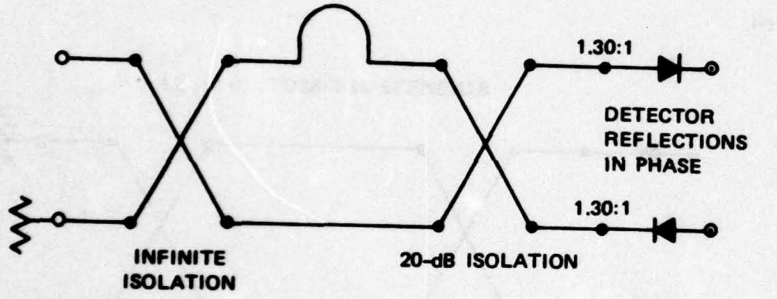

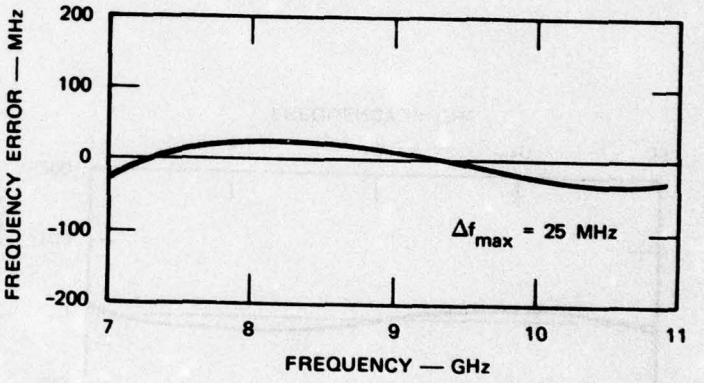

(d)

LA-4237-22

FIGURE 5 (Continued)

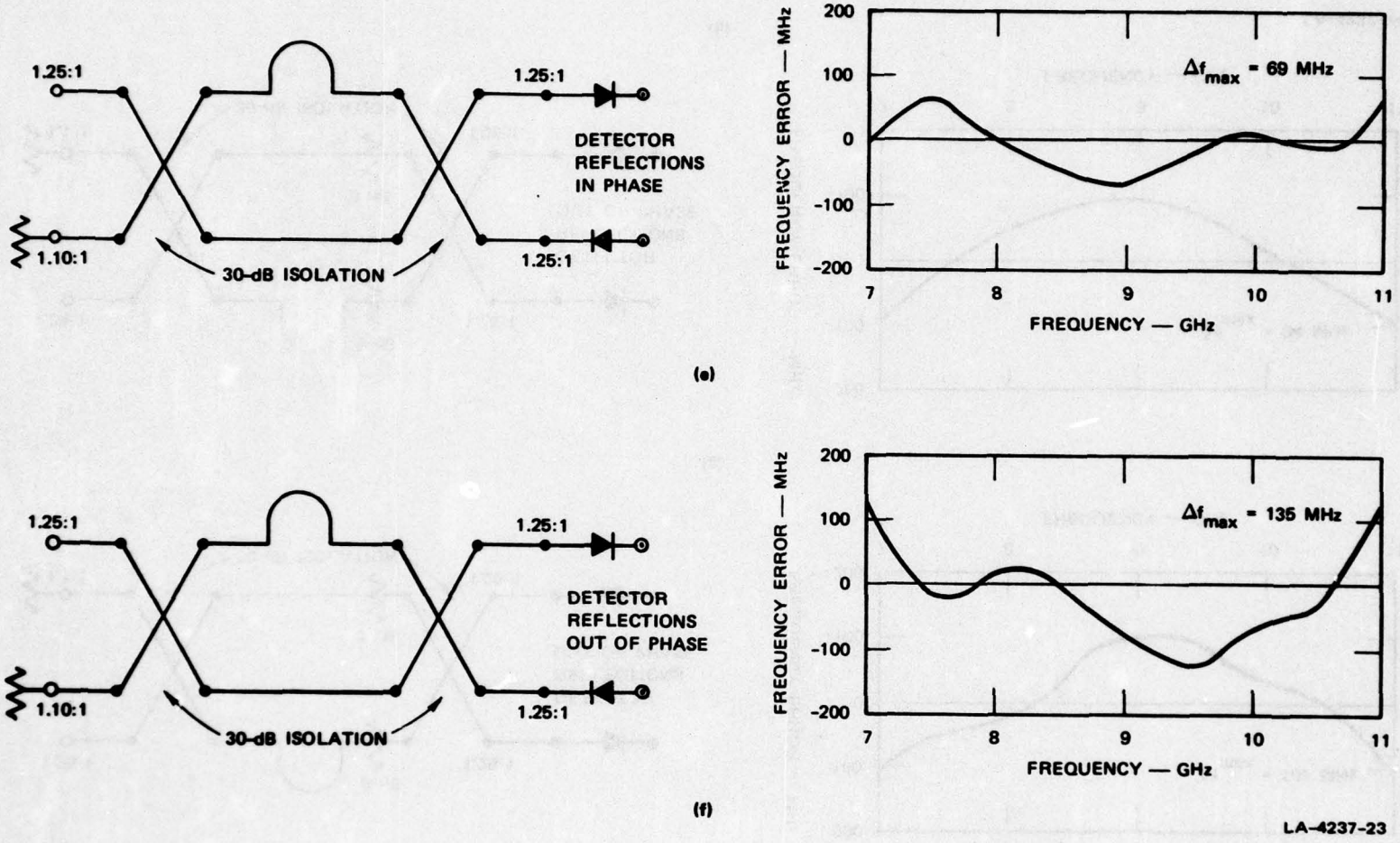

FIGURE 5 (Continued)

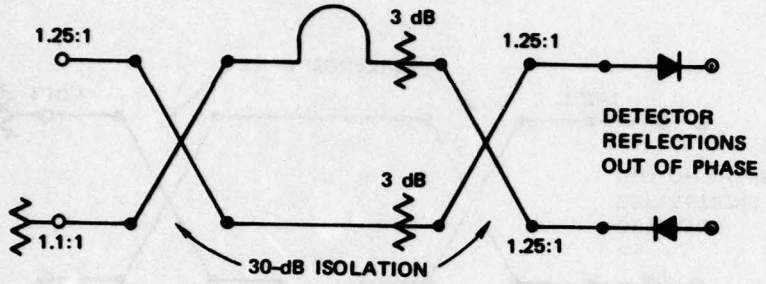

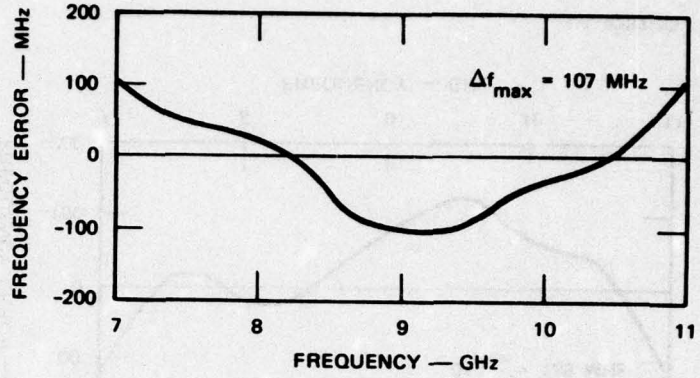

(g)

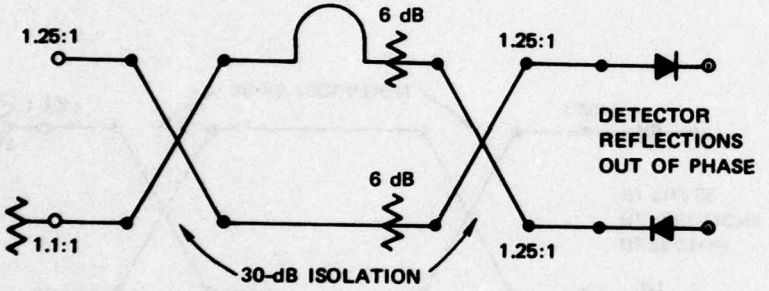

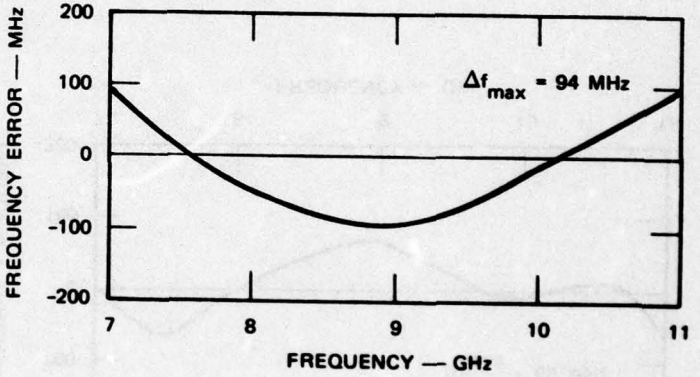

(h)

LA-4237-24

FIGURE 5 (Continued)

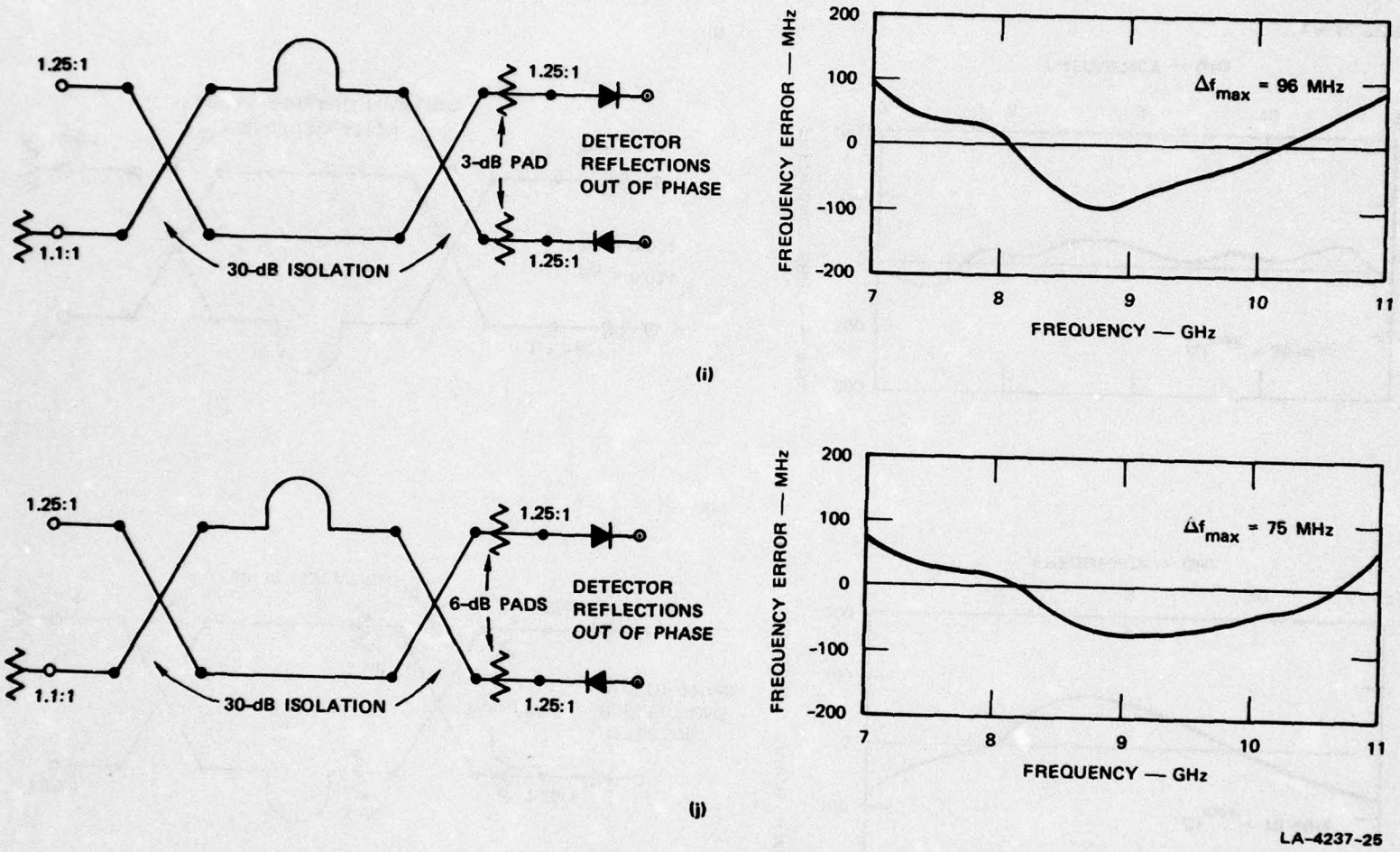

FIGURE 5 (Continued)

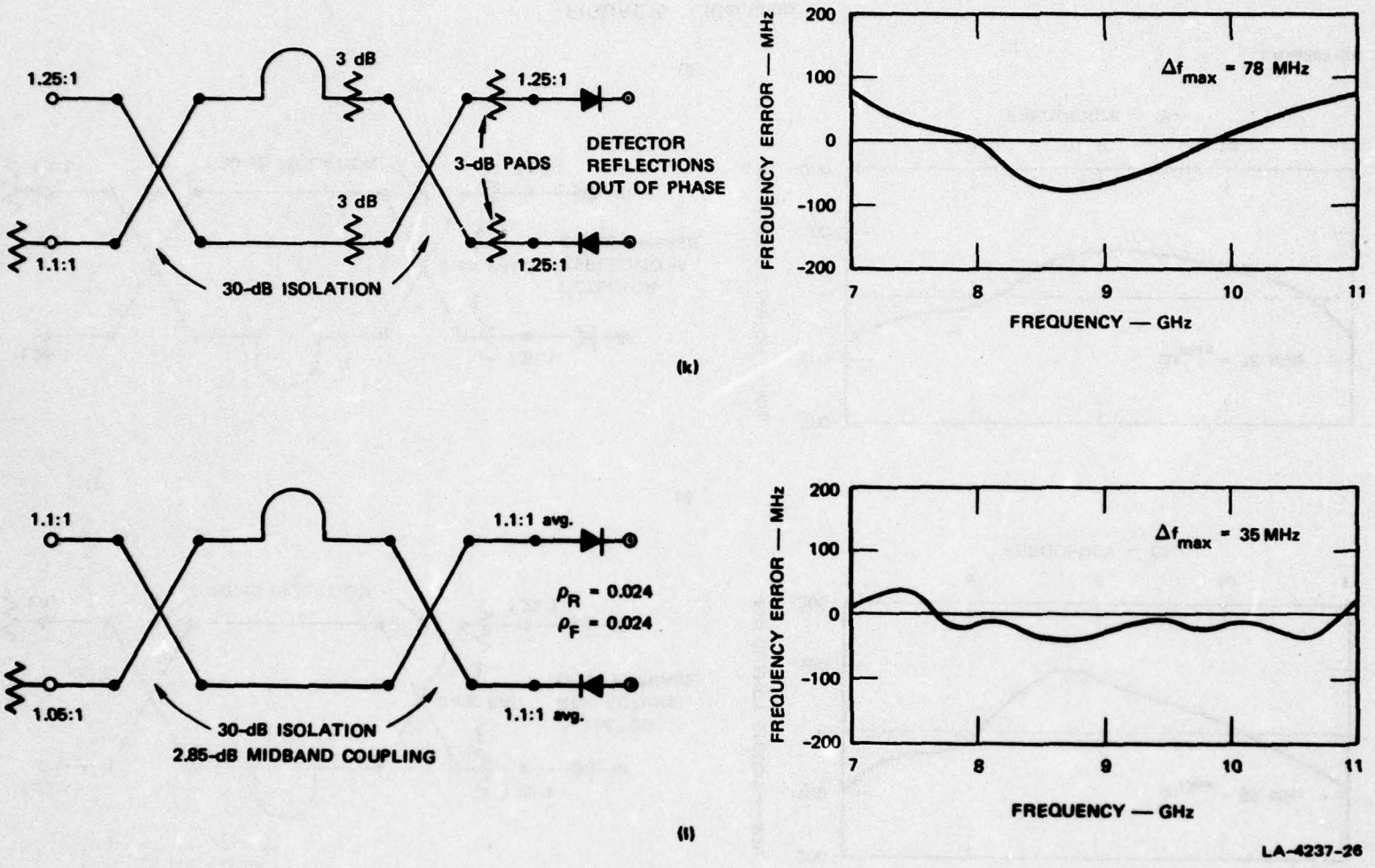

FIGURE 5 (Concluded)

The following cases show the effects of imperfections of the subcomponents, in particular the results of interacting VSWRs. The lines are assumed to be lossless and their lengths are representative of the actual device. Unless otherwise noted, the VSWRs are perfect and the couplers have 2.8 dB midband coupling. It was found that the phase angles of the reflection coefficients and of the coupler isolations have little or no effect on the maximum frequency error. Therefore only the VSWRs and the isolations in dB are indicated in the figures. Figures 5(c) and (d) show the effect of poor coupler isolation in combination with detector reflections. The frequency deviation was ±160 MHz for 20 dB isolation of the first hybrid, while the second hybrid was assumed to be ideal. By contrast, when the first hybrid was perfect and the second hybrid had 20 dB isolation, the frequency error was only ±25 MHz. These results were obtained for detectors with in-phase reflection coefficients (tracking of the detector VSWRs). Similar results were obtained for detectors with out-of-phase reflection coefficients. The different effects of the two couplers stem from the delay line between the two couplers. Interactions between the second coupler and the detectors occur symmetrically--i.e., whether the detectors have in-phase or out-of-phase reflection coefficients, the resulting mismatch losses of both detectors are in phase. Therefore, when the video amplifier takes the difference between the two detector output voltages, the mismatch losses cancel approximately. Exactly the opposite takes place for interactions between imperfect detectors and an imperfect first coupler. There, the net effect is a reduced mismatch loss at one detector and an increased mismatch loss at the other. This leads to a large periodic frequency error, whose periodicity can be traced readily to the distance between the first coupler and the detectors (half wavelength). Similar results are obtained for a discriminator with perfect couplers but imperfect detectors, internal load (ρ_4), and

input VSWR (ρ_1). In-phase detector reflections reappear at the input and interact with ρ_1. The resulting frequency error is caused mostly by the overall mismatch loss at the input of the discriminator. Out-of-phase detector reflections are channeled into the internal terminations. A poor match at that port causes very large periodic frequency errors. The periodicity corresponds to half of a wavelength between the detectors and the internal load. Figure 5(e) and (f) show the combined effect of finite reflection coefficients at all four ports in conjunction with good couplers (30 dB isolation). When the detector reflection coefficients were in phase, the frequency deviation was ±69 MHz, but when the detector reflection coefficients were out of phase, the frequency error increased to ±135 MHz.

Attenuators can be used to reduce the interaction between the components, and this means was also investigated. Representative configurations and results are shown in Figures 5(f) through (k). The results indicate that pads between the detectors and the output hybrid are the most effective method for improving the linearity. Several other configurations were evaluated, and it was determined that in every case additional padding between either the input and output hybrids or between the output hybrid and the detectors improved the linearity over that of the nonpadded configuration. The optimum position for the attenuators varied, depending on the actual component parameters.

Finally, Figure 5(ℓ) shows the circuit parameters and results of the analysis for a general case. The line lengths correspond to those actually used in the circuit. The detector reflection coefficients were assumed to track within a circle of radius $\rho_R = 0.024$, and the frequency-dependent tracking error was characterized by $\rho_F = 0.024$ [see Eq. (12)]. These parameter values are considered to be those achievable with very good components. Therefore the resulting frequency

error for this general case is an indication of the performance that can be achieved in practice with a microwave line discriminator.

The computer analysis clearly revealed the most sensitive components of the discriminator. It helped set development priorities and define specification goals for the individual subcomponents in order to obtain a certain frequency accuracy. The major points are as follows, in order of decreasing importance:

(1) The detectors should be well matched. The remaining reflection coefficients should track with frequency and be constant over the operating RF power range.

(2) Of the two hybrids, the input hybrid is the most critical for linearity as far as isolation is concerned.

(3) The internal termination should be well matched.

(4) The connecting line lengths between the components should be kept as short as possible.

(5) Linearity can be improved by isolation of the components through the use of pads at the expense of decreased frequency sensitivity.

(6) The circuit should be realized with minimum conductor losses.

(7) The midband coupling and center frequency of the couplers should be close to the design values: however, they are of secondary concern compared with the coupler isolation.

(8) Detectors operating in the linear instead of the square-law mode do not improve the linearity noticeably, because most errors are caused by interacting VSWRs. The latter are unaffected by the diode operating mode. However, a higher input signal level will increase the video output voltage and the signal-to-noise ratio (SNR).

The computer-model results were later fully confirmed by the experimental work. Not included in the computer model are any errors

due to nonlinear effects such as harmonics generated internally in the detectors. Those have to be analyzed separately.

IV DISCRIMINATOR PERFORMANCE

From the outset of the program it was clear that the components of the discriminator had to perform extremely well, if the goal of a frequency error of less than ±10 MHz was to be achieved. Therefore, before detailed results of the computer analysis were available, efforts were initiated to develop 3-dB quadrature hybrids, detectors, attenuators, and terminations with performances better than those customary for MIC circuits. These development efforts are described in more detail in Section V. The first microstrip discriminator (Model 1) was assembled within six months after the start of the program. It is shown in Figure 6. The photograph shows the two quadrature hybrids, the delay line, and the two multiplexer-detector circuits. Each detector contains two diodes, as will be explained later.

The discrimnator circuit is contained on a 1-inch-by-1-inch sapphire substrate with a thickness of 0.010 inch, and is mounted in a case that also contains the video amplifier. Initial measurements were performed with a manual setup. It became apparent immediately that a more accurate and efficient measurement procedure was required, because adjustments of the bias currents of the four detector diodes can be used to optimize the linearity of the response. To make full use of this possibility, an accurate and essentially real-time measurement system was required. Such a system was put together by adapting SRI's Hewlett-Packard Automatic Network Analyzer (ANA). This system simulates an almost perfect limiter and made possible measurements with an accuracy of less than ±16 MHz. A detailed description of the automated measurement system is given in Section VI. All measurements reported here were taken with this system.

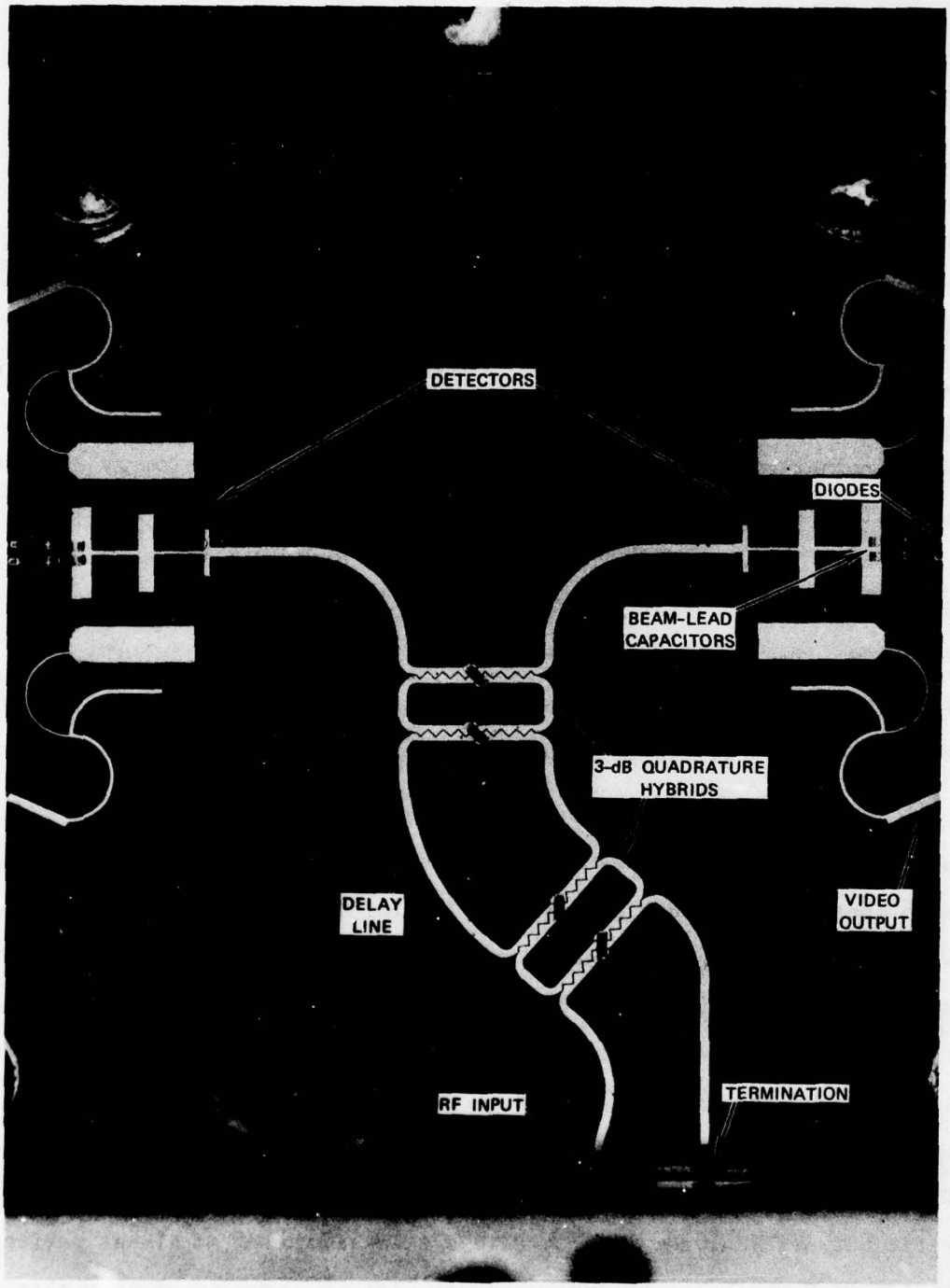

LA-4237-12R

FIGURE 6 PHOTOGRAPH OF THE FREQUENCY-DISCRIMINATOR MIC CIRCUIT (Model 1)

The measured performance of the first discriminator (Model 1), which includes a 20-dB video amplifier, is shown in Figure 7. The top curve shows the output voltage versus input frequency. The second curve shows the deviations of the discriminator response from a best straight-line approximation; the results are expressed in frequency error, not in error voltage. The approximation is made in a Chebyshev sense, which minimizes the maximum frequency error. A second discriminator similar to the first discriminator circuit but including two 3-dB attenuators was fabricated and tested. Figure 8 is a photograph of this discriminator (Model 1a), and the measured performance of this unit is presented in Figure 9.

Both discriminators exhibit a rather smooth frequency response. The small ripples superimposed on the generally parabolic response correspond to a frequency error of about ±20 MHz. Overall, the curve of output voltage with frequency has a constant curvature that is caused by circuit losses. This effect was discussed previously [Figure 5(b)] and follows directly from Eq. (6), but its importance was not realized until the measurements on the first two discriminators revealed its existence. From the measured data it was found that the observed curvature corresponds to a loss increase of nearly 2 dB over the frequency range 7 to 11 GHz. All the observed curvature is interpreted to have its origin in frequency-dependent losses, although some portion of the curvature may have a different origin. To compensate for this increase in loss, one could build a limiter with a complementary gain slope to precede the discriminator. Also, a purely passive gain-shaping network can be added at the input of the discriminator that converts a flat limiter output into a sloped output. Such a network will have a loss that is maximum at 7 GHz and that decreases with frequency so that at 11 GHz the loss approaches zero as closely as possible. The net effect is that the total power delivered to the two detectors is

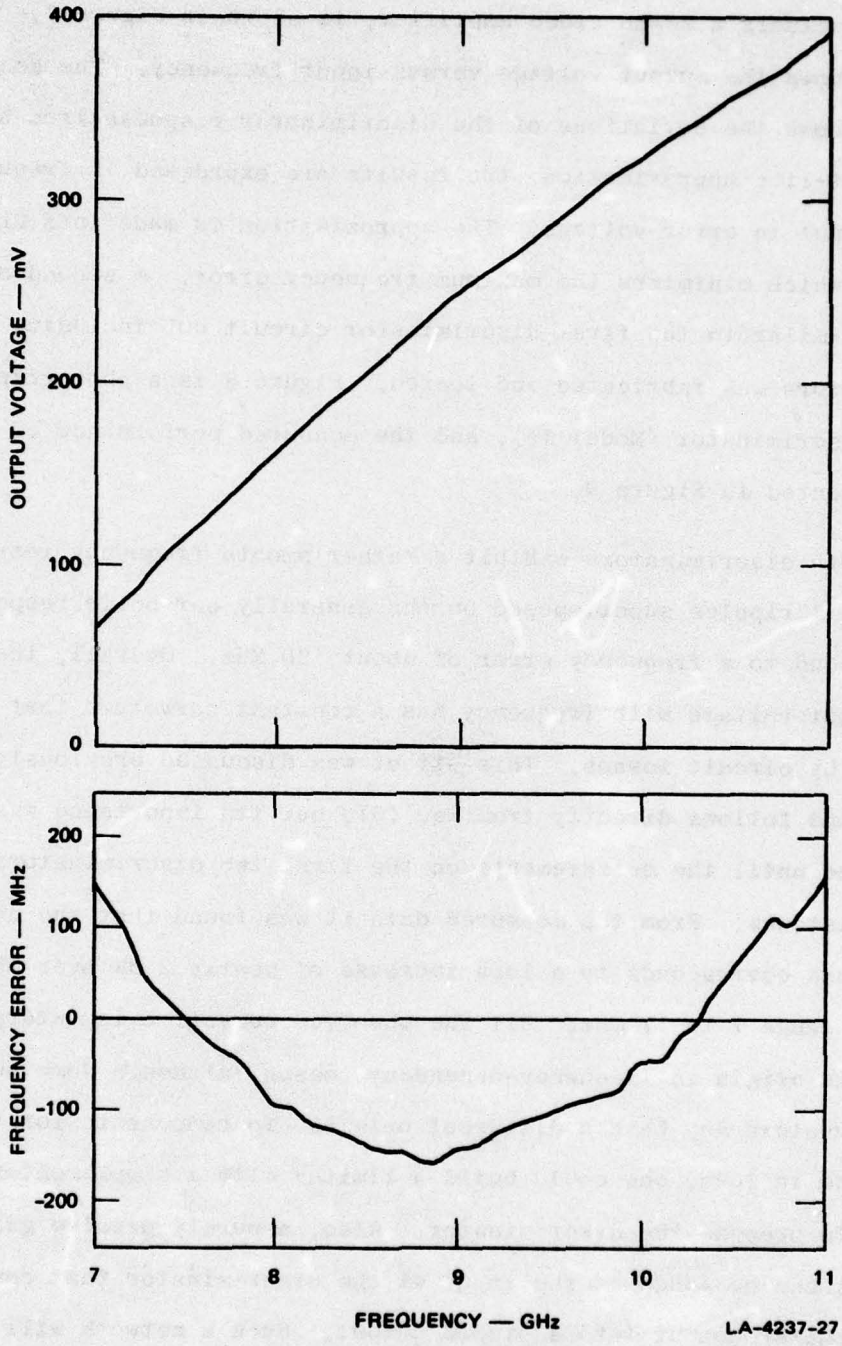

FIGURE 7 OUTPUT VOLTAGE AND FREQUENCY ERROR OF DISCRIMINATOR, MODEL 1

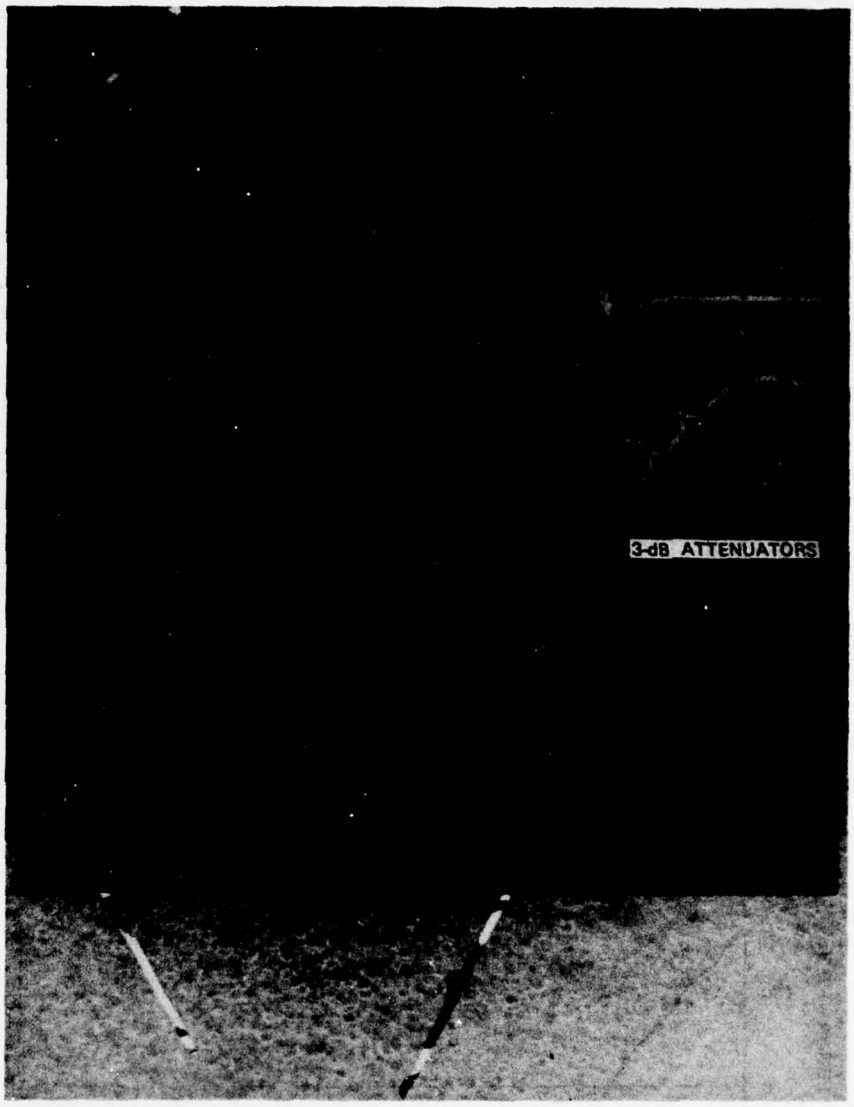

LA-4237-28

FIGURE 8 PHOTOGRAPH OF THE FREQUENCY-DISCRIMINATOR MIC CIRCUIT (Model 1a)

independent of frequency and is equal to or less than that of the uncompensated discriminator at the frequency of greatest loss--i.e., at 11 GHz. Therefore, the compensated discriminator has a reduced output voltage swing, as will be shown later. Fortunately the required insertion-loss function of the shaping network is almost linear in dB with frequency, and several suitable designs are available. These are discussed further in Section V-D.

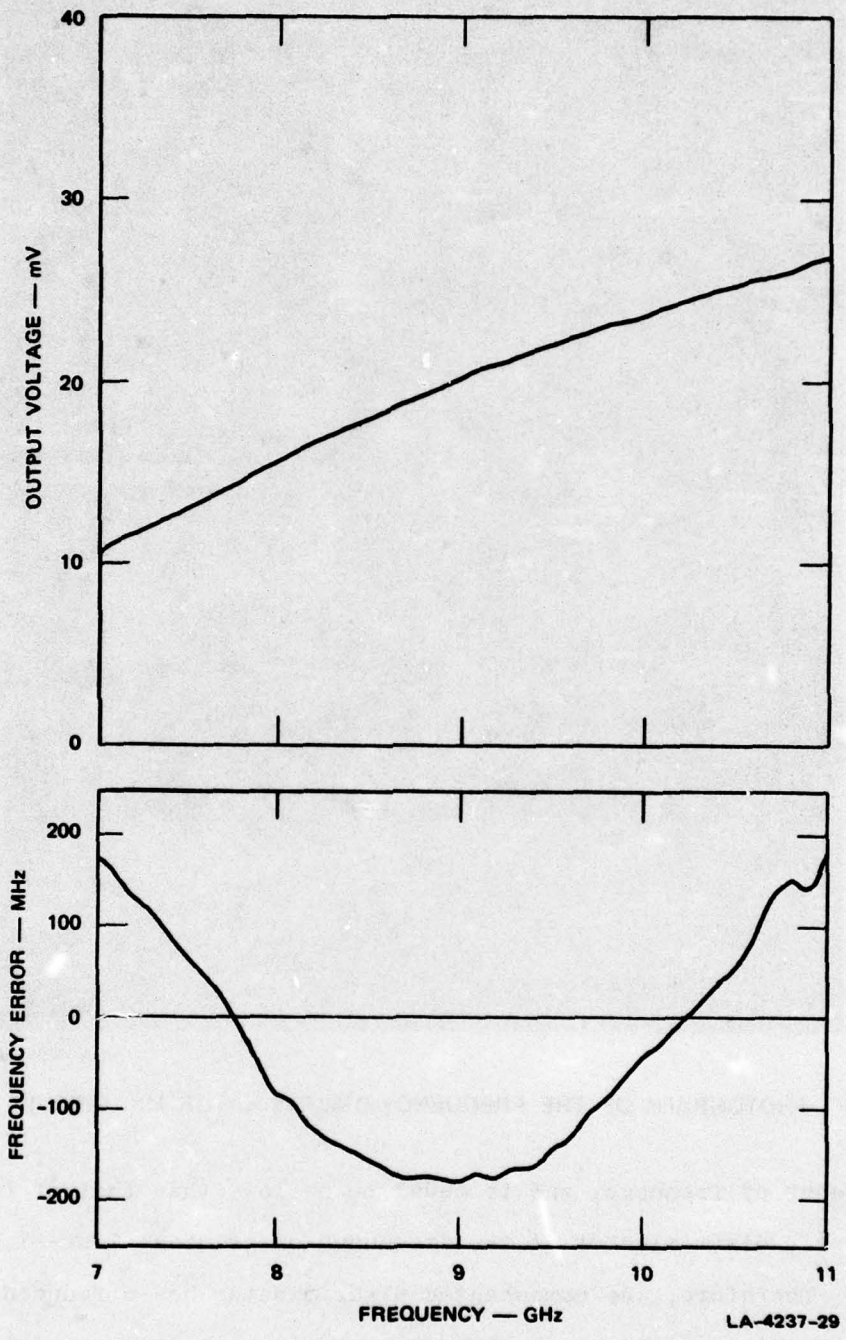

FIGURE 9 OUTPUT VOLTAGE AND FREQUENCY ERROR OF DISCRIMINATOR, MODEL 1a

The error response in Figure 9 shows a greater-than-normal ripple at 10.7 GHz. When this circuit was first tested it was believed that the ripple was a deficiency of that particular circuit. However, subsequent discriminator units all showed a "glitch" in the response at 8.8 GHz and another very pronounced one around 10.5 GHz. Several identical discriminator circuits were fabricated and tested, and all exhibited "glitches" to some degree at those two frequencies. A typical response is shown in Figure 10, where the circuit was tuned for the smallest possible error from a smooth parabolic response. A different and probably more correct tuning would have resulted in a smooth curve up to 10.4 GHz and a sharp peak between 10.4 and 10.9 GHz. The source of these anomalies was eventually traced to harmonic absorption. The detectors are designed to reflect internally generated harmonics back into the diodes. However, in the initial detector circuit the third harmonics saw a narrowband match around 26.5 GHz and 31.5 GHz, which resulted in a net drop in the detector efficiency at the corresponding fundamental frequencies, and caused the "glitches" in the discriminator response. To solve this problem a complete redesign of the harmonic filters for the detector was required. A new detector circuit was fabricated and incorporated into the discriminator circuit (Model 2). No signs of harmonic absorption were evident in tests of the new circuit.

A final model of the frequency discriminator was realized by combining the improved discriminator circuit with a shaping network. The shaping network fabricated on a separate substrate was mounted in front of the basic discriminator circuit substrate as shown in Figures 11 and 12. Details of the circuits will be given in Section V. The improved and uncorrected responses of the final discriminator model are shown in Figure 13. Improved linearization has been achieved at the expense of a decreased sensitivity. The maximum error of ±32 MHz is not quite as good as might be expected from Figure 7, where small

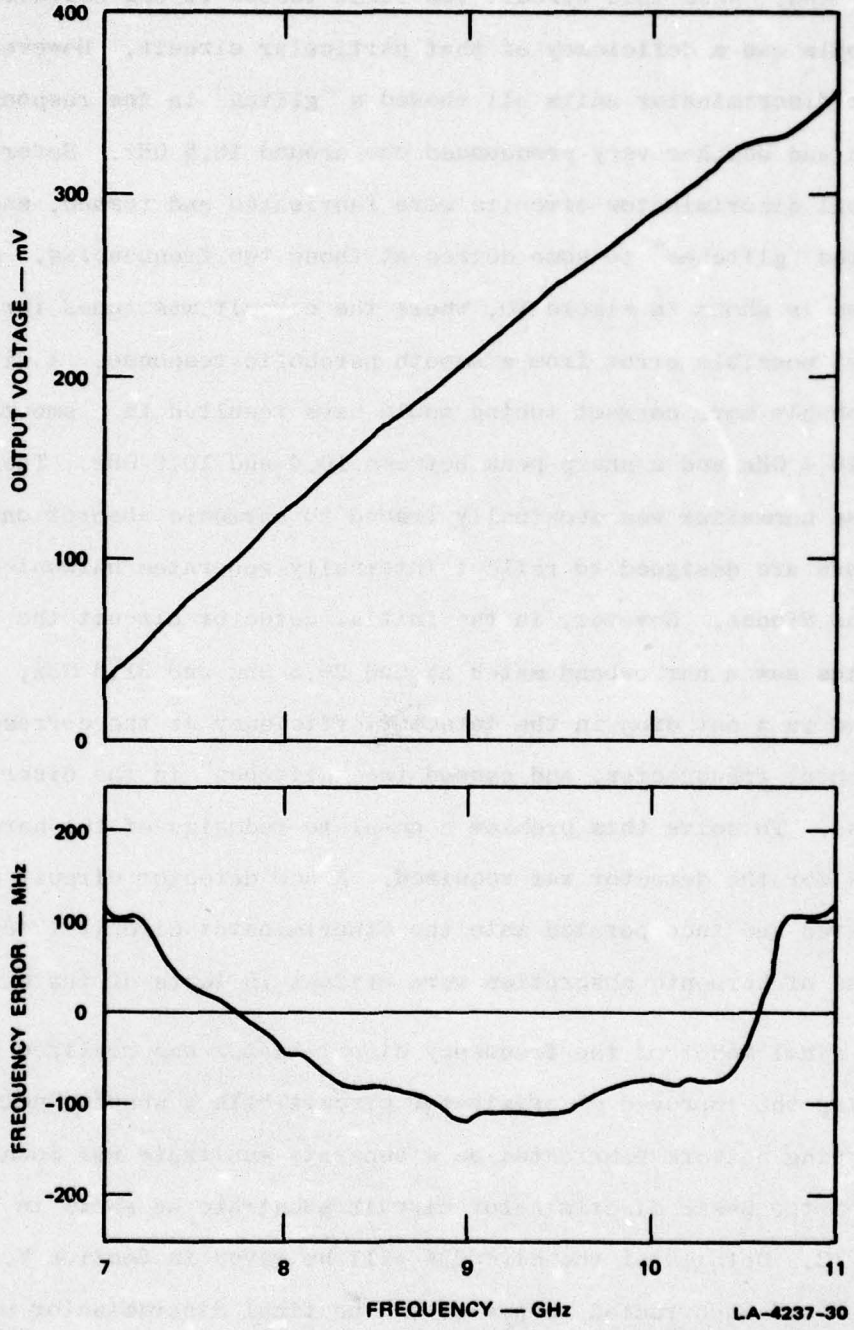

FIGURE 10 OUTPUT VOLTAGE AND FREQUENCY ERROR OF DISCRIMINATOR, MODEL 1 (SN 3-76-2)

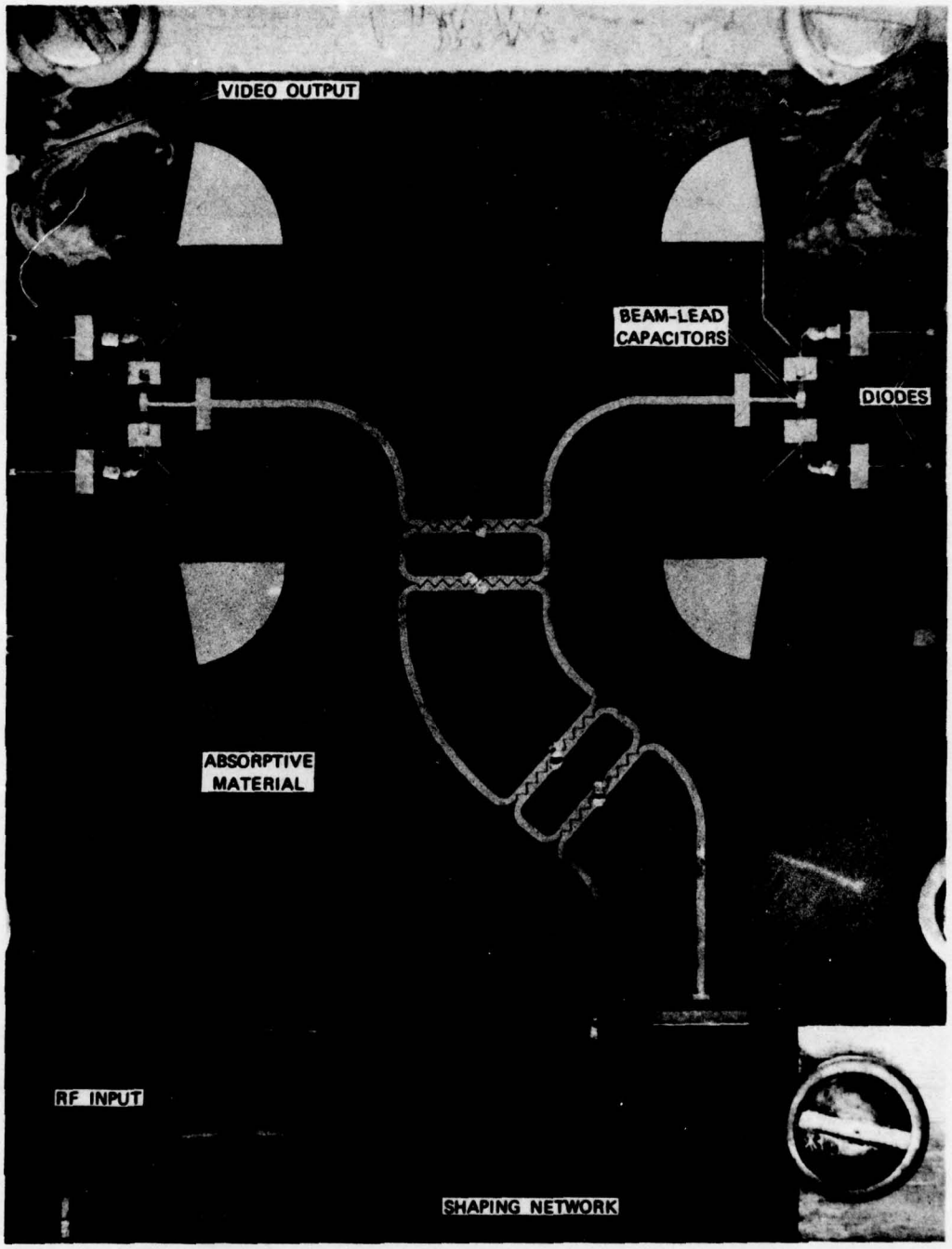

LA-4237-31

FIGURE 11 PHOTOGRAPH OF THE FREQUENCY-DISCRIMINATOR MIC CIRCUIT WITH SHAPING NETWORK (Model 2)

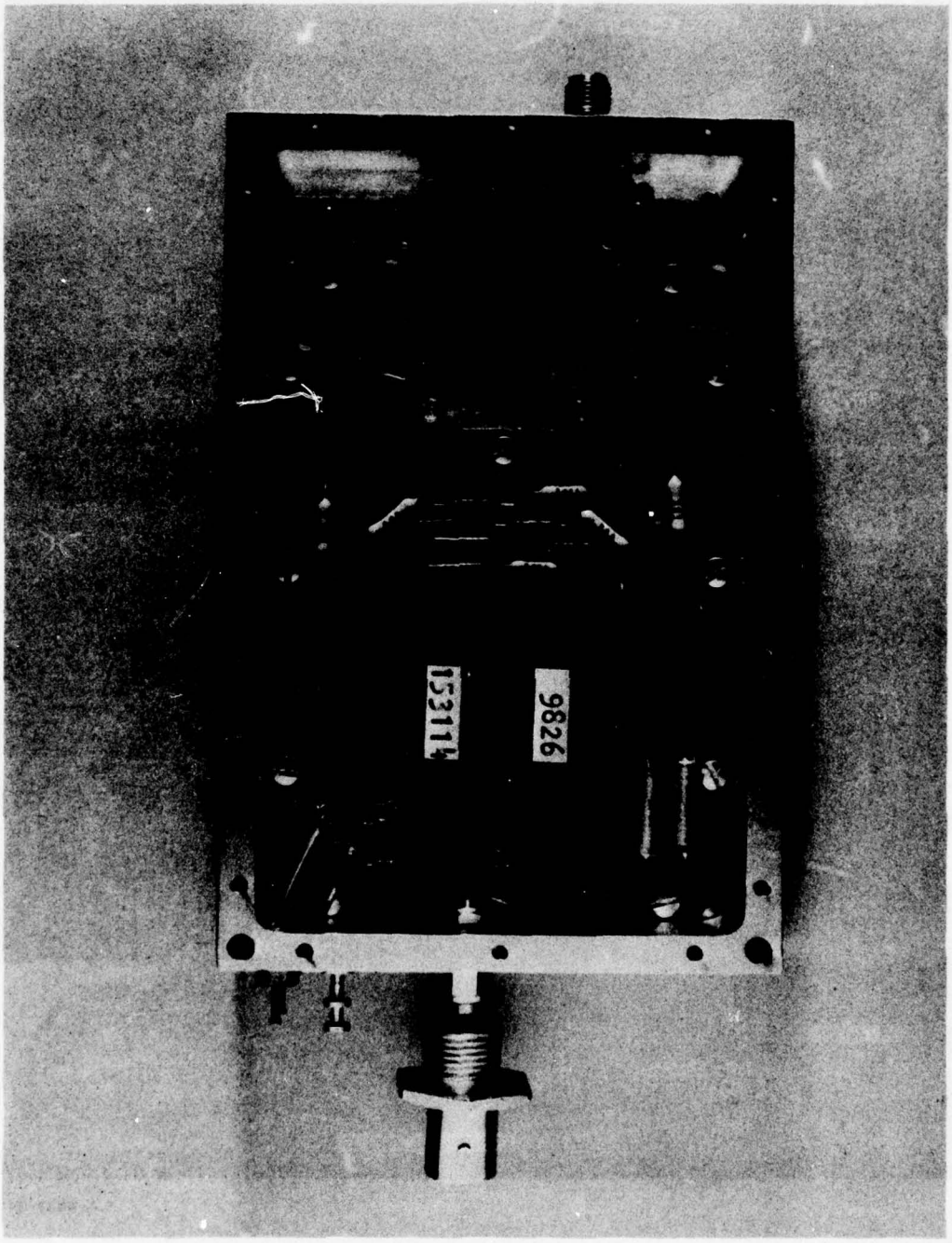

LA-4237-32

FIGURE 12 OVERALL VIEW OF THE FREQUENCY DISCRIMINATOR

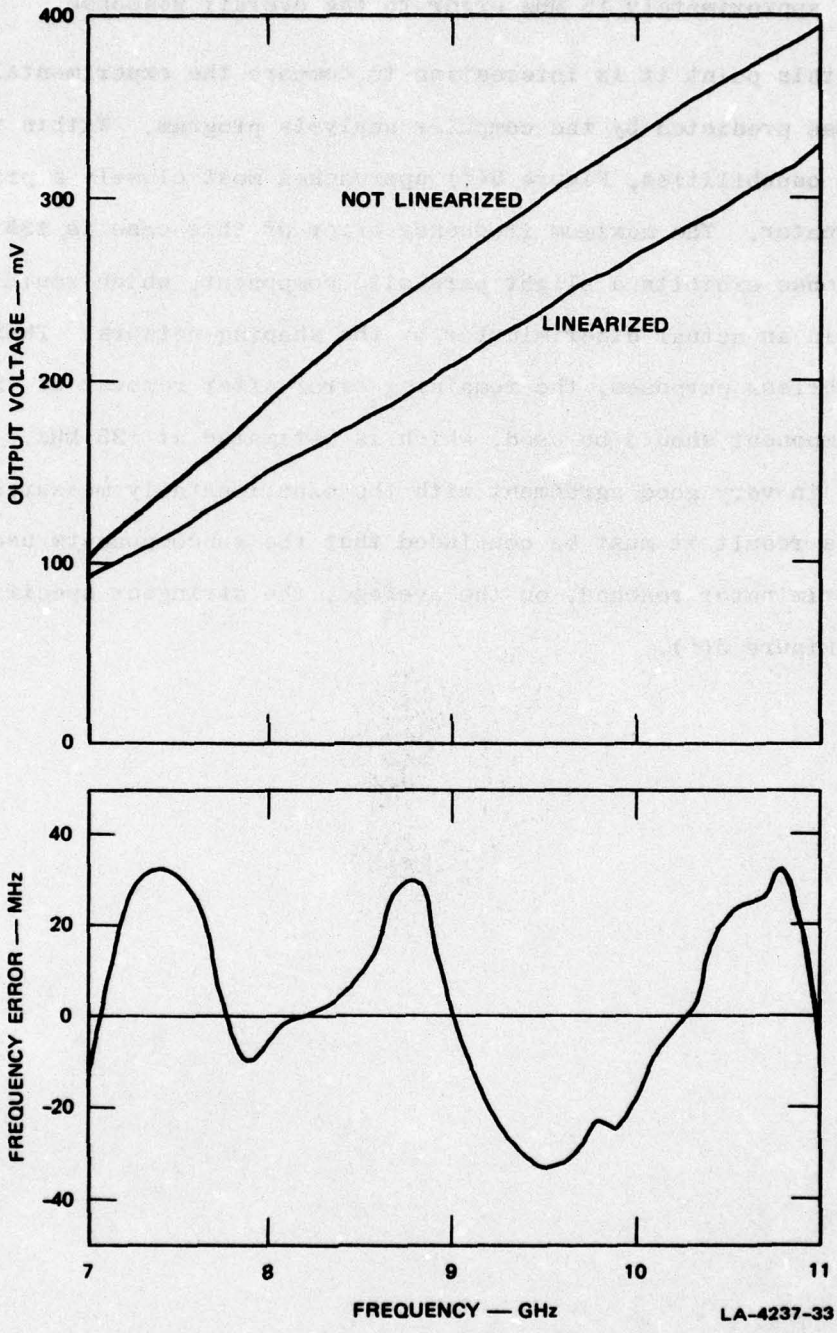

FIGURE 13 OUTPUT VOLTAGE AND FREQUENCY ERROR OF LINEARIZED DISCRIMINATOR, MODEL 2

ripples of only ±20 MHz were observed. The linearization is not perfect and adds approximately 15 MHz error to the overall response.

At this point it is interesting to compare the experimental results with those predicted by the computer analysis program. Within the latter's capabilities, Figure 5(ℓ) approaches most closely a practical discriminator. The maximum frequency error of this case is ±35 MHz. The response exhibits a slight parabolic component, which would be removed in an actual discriminator by the shaping network. Therefore, for comparison purposes, the remaining error after removal of the parabolic component should be used, which is estimated at ±25 MHz. This value is in very good agreement with the experimentally measured error. From this result it must be concluded that the subcomponents used in the discriminator reached, on the average, the stringent specifications used in Figure 5(ℓ).

V COMPONENT DEVELOPMENT

A. Quadrature Hybrid

1. MIC Quadrature Hybrid Evaluation

Three different quadrature hybrids that can be realized in planar MIC form were evaluated for application in the discriminator. These are the wiggly coupler,[3] the Lange interdigital coupler,[4] and the hybrid slotline coupler,[5] as shown in Figures 14(a) through 14(c). Each coupler is drawn approximately to scale for a center frequency of 9 GHz and an assumed substrate thickness of 10 mils for the configurations in Figures 14(a) and 14(c), and a substrate thickness of 20 mils for the configuration of Figure 14(b). Two major problems exist in the construction of a broadband MIC 3-dB quadrature hybrid. The first is that the velocities of the even and odd modes in the coupled microstrip lines are unequal. This effect degrades the coupler directivity and VSWRs. The second problem is that it is difficult to achieve less than 6 dB coupling with an edge-coupled line. A third but less critical problem with planar couplers is that crossovers in the coupling arms are required.

The "wiggly" coupler solves the first problem by lengthening the coupling gap, thereby slowing down the odd mode. The second problem is solved by cascading two 8.34-dB "wiggly" couplers to obtain a 3-dB coupler. The Lange coupler solves the unequal-velocity problem and the need for tight coupling by using narrow interdigitated fingers. The hybrid branchline coupler is a new approach to 3-dB quadrature hybrids. A slotline in the ground plane that is open-circuited at the ends lies symmetrically underneath the branch arm of a simple H-shaped circuit

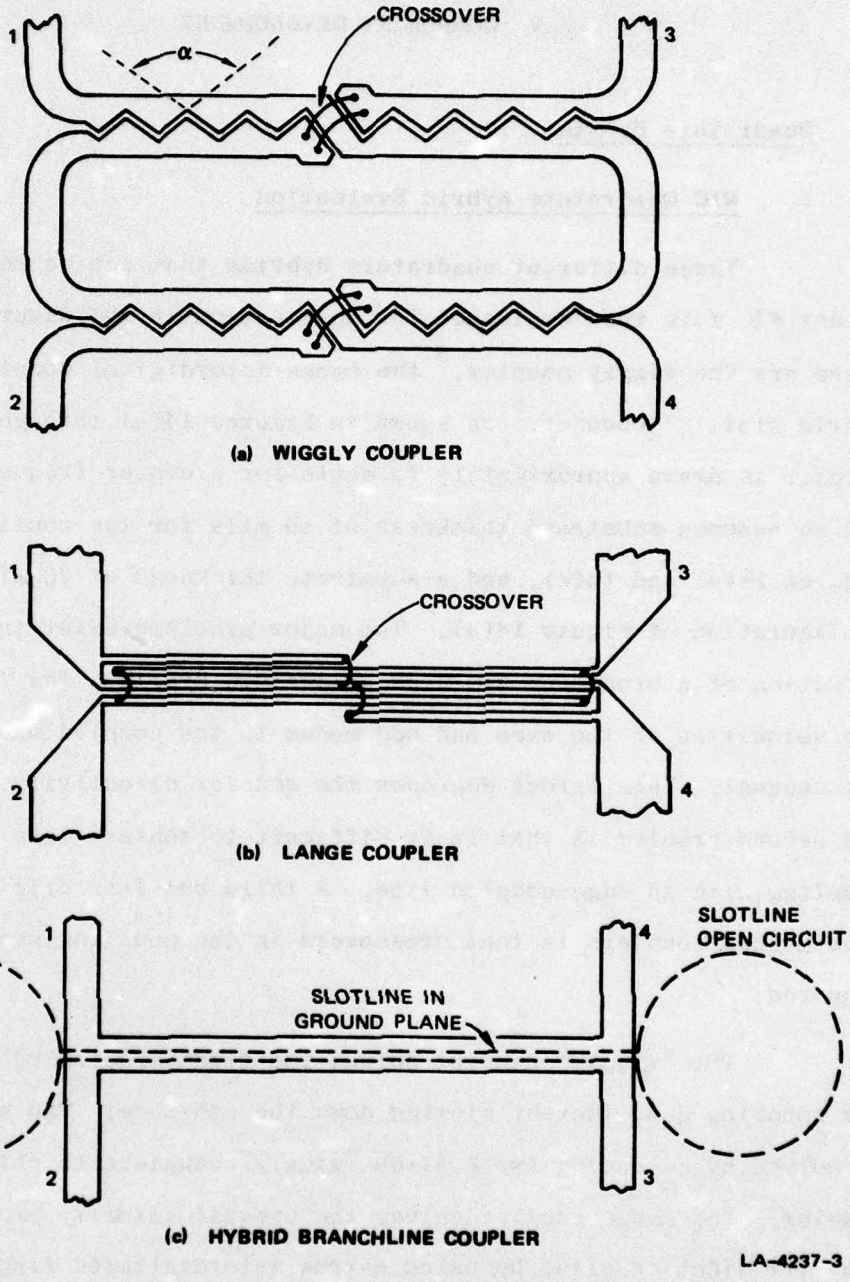

FIGURE 14 THREE POSSIBLE MIC QUADRATURE HYBRIDS

on the top of the substrate. With perfect open circuits for the slotline, this hybrid is exactly equivalent to the other two hybrids. However, the circular cutouts at the ends of the slotline represent only a modest approximation to an open circuit, and the bandwidth of this hybrid is less than that of a perfect parallel-coupled-line hybrid.

The major advantages and disadvantages of the three couplers are listed in Table 1. An analysis of these couplers indicated that the "wiggly" coupler was the most promising approach.

2. "Wiggly" Coupler Development

An 8.08-dB wiggly coupler was designed and tested using design information developed under previous Navy contracts.* This coupler constitutes one-half of a 2.8-dB coupler. A midband coupling of 2.8 dB was found to be the optimum value for the discriminator. Sapphire substrate was selected because it has very good electrical and mechanical properties. A thickness of 0.010 inch was used in order to obtain a coupler with a favorable aspect ratio (length of coupler compared with width of lines) to minimize parasitic junction effects.

Experimental models of the coupler 25 times lower in frequency (center frequency 360 MHz) were used during the initial development stages. For modeling purposes, a dielectric substrate with $\epsilon_r = 10$ and a thickness of 0.250 inch was selected.† Models of the 8.08-dB couplers were optimized by adjusting the coupling gap, the coupler length, and

---

*Contract N00123-74-C-1957 from Naval Electronics Laboratory Center, San Diego, California, and Contract N00014-72-C-0283 from Naval Research Laboratory, Washington, D.C.

†3M Company, HiK 707L.

Table 1

COMPARISON OF THREE DIFFERENT MIC 3-dB QUADRATURE HYBRIDS

	Wiggly Coupler	Lange Coupler	Hybrid Branchline Coupler
Advantages	Excellent velocity equalization. Only two crossovers needed. Reasonable coupling gap.	3-dB coupling realizable in one section. Simple geometry.	3-dB coupling realizable in one section. Very simple geometry. No crossovers. Excellent performance achievable.
Disadvantages	Relatively large because two 8.3-dB couplers have to be cascaded to obtain a 3-dB hybrid.	Cannot be built on 10-mil substrate because the fingers would be too narrow. This leads to an unfavorable aspect ratio of the coupler (more pronounced junction effects). The wires are difficult to bond, and adhesion problems of the gold on the substrate can lead to production difficulties.	No crossover possible. Through arm and coupled arm are on opposite sides of the coupler. The slotline open circuits can only be approximated, which reduces the bandwidth of the coupler. Two-sided etching of the substrate required, with its possible registration problem. Cavity in ground plane underneath slotline required.

the wiggle angle α [see Figure 14(a)]. The best results obtained on these models included a VSWR of less than 1.1:1 at all four ports, isolation of better than 31 dB, and a coupling of 0.08 dB within the theoretical value. Subsequently a low-frequency model and two actual-size models of a 2.8 dB coupler were fabricated and tested. Measured results for the coupling, isolation, and VSWR for the first actual-size coupler are shown in Figure 15. This coupler is overcoupled and centered too high in frequency. The ripples in the VSWR result from interactions between the VSWR of the coupler itself and the VSWR of the transitions between the substrate and the coaxial connectors. It is estimated that of the total VSWR, one-half is due to the coupler itself and therefore its maximum VSWR is approximately 1.2:1. The isolation and the VSWR correlate closely, as predicted theoretically. The isolation is better than 30 dB over a large portion of the band.

A second actual-size coupler was fabricated with appropriate changes to obtain the proper coupling and center frequency. Due to overetching, the gap between coupled lines was too wide, and coupling was too weak. The VSWR and the isolation were slightly improved compared with the first model. Based on the results of the two models, the dimensions for the desired coupler were determined, including a gap width of 1.65 mil. Instead of testing a third version of the coupler separately, a coupler with final dimensions was integrated directly on the same substrate with the complete discriminator circuit. Judging by the results obtained on the completed discriminator, the coupler performed as expected with a coupling of 2.8 ± 0.2 dB and an isolation of 25 dB or better.

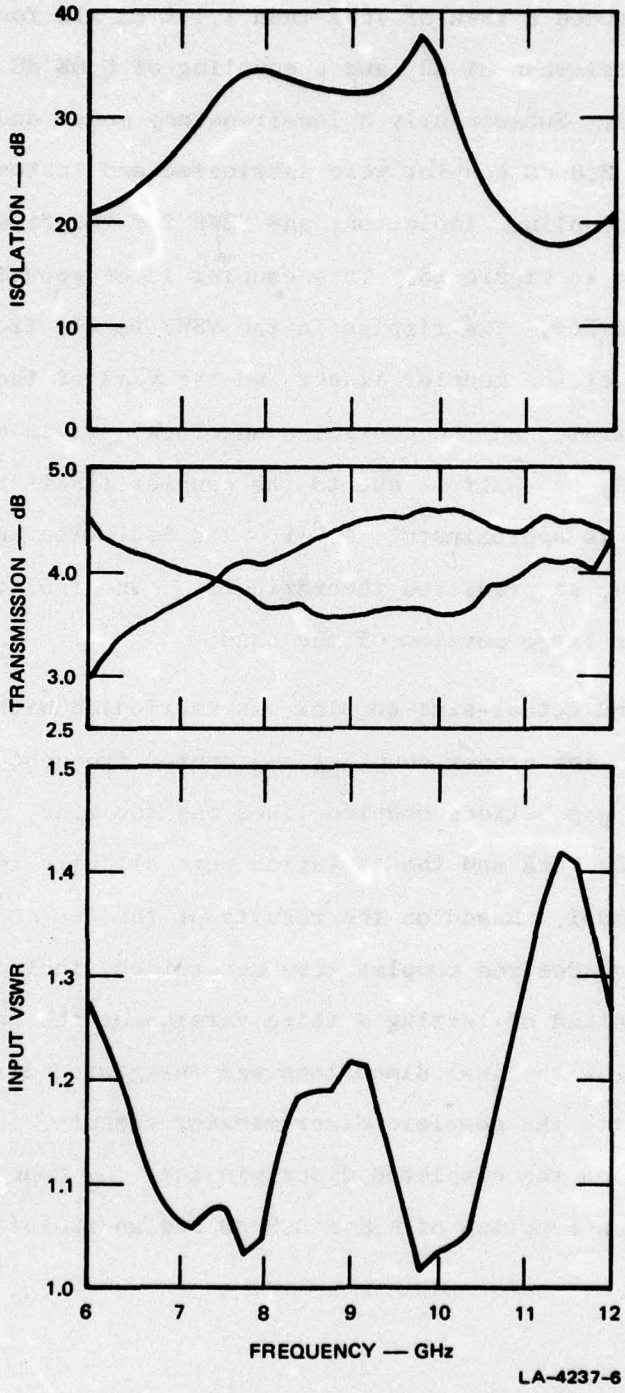

FIGURE 15 MEASURED CHARACTERISTICS OF 3-dB QUADRATURE HYBRID

B. Detectors

1. Circuits for Detector and Multiplexer

The design of the detector circuit was chosen to provide a flat response, low VSWR characteristics, and controlled impedances for the higher harmonics that are generated in the detector diode. The basic detector circuit is shown in Figure 16. It consists of four

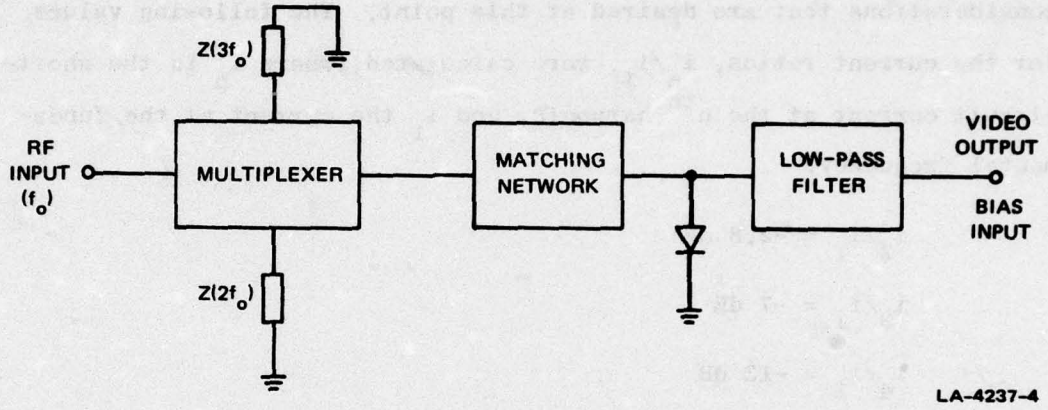

FIGURE 16 SCHEMATIC OF DETECTOR CIRCUIT

parts--the Schottky-barrier detector diode, an RF matching network, a multiplexer to terminate the higher harmonics, and a low-pass filter for the video signal, which also allows for the biasing of the diode. It is necessary to bias the diode to obtain an average junction resistance, R_j, suitable for matching the diode at the RF terminal. The choice for R_j is a function of the generator impedance, in this case 50 ohms, and the parasitic elements of the diode. The latter become part of the matching network, which can only be realized if R_j is comparable to the reactance of the diode junction capacitance.

The multiplexer is essential to prevent the harmonics that will be generated in the detectors from reentering the passive portion of the discriminator. There they could be reflected back again into

the detectors with rapidly changing phase, resulting in strong and closely spaced ripples. To demonstrate the importance of the harmonic filtering, the expected harmonic signal levels in the detectors were estimated. In the present system, each detector operates at a nominal signal level of -10 dBm. The calculations are based on a match at the RF port and a short-circuit for all harmonics. The latter condition is not exactly met, but is sufficiently accurate for the order-of-magnitude considerations that are desired at this point. The following values for the current ratios, i_n/i_1, were calculated, where i_n is the short-circuit current at the n^{th} harmonic, and i_1 the current at the fundamental frequency:

$$i_2/i_1 = -2.8 \text{ dB}$$

$$i_3/i_1 = -7 \text{ dB}$$

$$i_4/i_1 = -13 \text{ dB} \quad .$$

These numbers clearly demonstrate that strong harmonic signals are present in the detector and harmonic filtering is definitely required.

Three design approaches were considered for the multiplexer: a true multiplexer, an absorptive harmonic filter, and a filter that reactively terminates the harmonics. In a true multiplexer a low-pass filter passes the RF signal to the diode, and the harmonics (primarily the second and third) are filtered out with a high-pass (or bandpass) filter and resistively terminated. Because this approach required filters with high selectivities and because high-pass or wideband bandpass filters are difficult to realize in microstrip, it was not used. Absorptive harmonic filters are frequently employed to suppress harmonic outputs from TWTAs. These filters generally use resistively loaded waveguides that are below cutoff in the passband of the filter. When side-coupled to the main guide, these waveguides absorb power above the

cutoff, which is adjusted to coincide with the beginning of the stopband of the filter. A microstrip realization of this type of filter appears impossible at the present time. In the third approach the harmonics are reactively terminated (e.g., in a short or an open) and are therefore prevented from propagating back into the RF input. The rectifying properties of the diode depend on the magnitude of the reactive termination for the higher-harmonic signals. Therefore, the reactance as seen by the diode junction at the harmonic signals must remain as constant as possible. This requires filters that are connected directly to the beam-lead Schottky-barrier diode. This last solution is the easiest to implement in microstrip and was therefore selected for further evaluation.

Three circuit approaches to the design of a detector with reactively terminated harmonics are shown in Figures 17(a) through 17(c). In all three designs the matching network is an integral part of the required filters. The circuit in Figure 17(a) uses a single diode. The low-pass filter LP1 matches the diode in the 7-to-11-GHz band but stops all harmonics at least up to 33 GHz. LP2 is used to extract the video signal. A detailed design study for this circuit showed that a high-order filter for LP1 would be required in order to stop the lowest second-harmonic signal sufficiently. Also, the reactance presented to the diode at the second harmonic changes rapidly over the operating band, which makes this approach unsuitable.

The circuits in Figures 17(b) and 17(c) make use of an anti-parallel pair of diodes. This arrangement has the advantage that any even harmonics generated in the two diodes will cancel each other at the common junction at the RF input side. Therefore, the requirements for the filter LP1 in the circuits of Figures 17(b) and 17(c) can be relaxed, because the filter has to stop only the third harmonics starting at 21 GHz. These two circuits are duals of each other. In Figure 17(b) the filter LP2 is required to present a short circuit to the diodes from

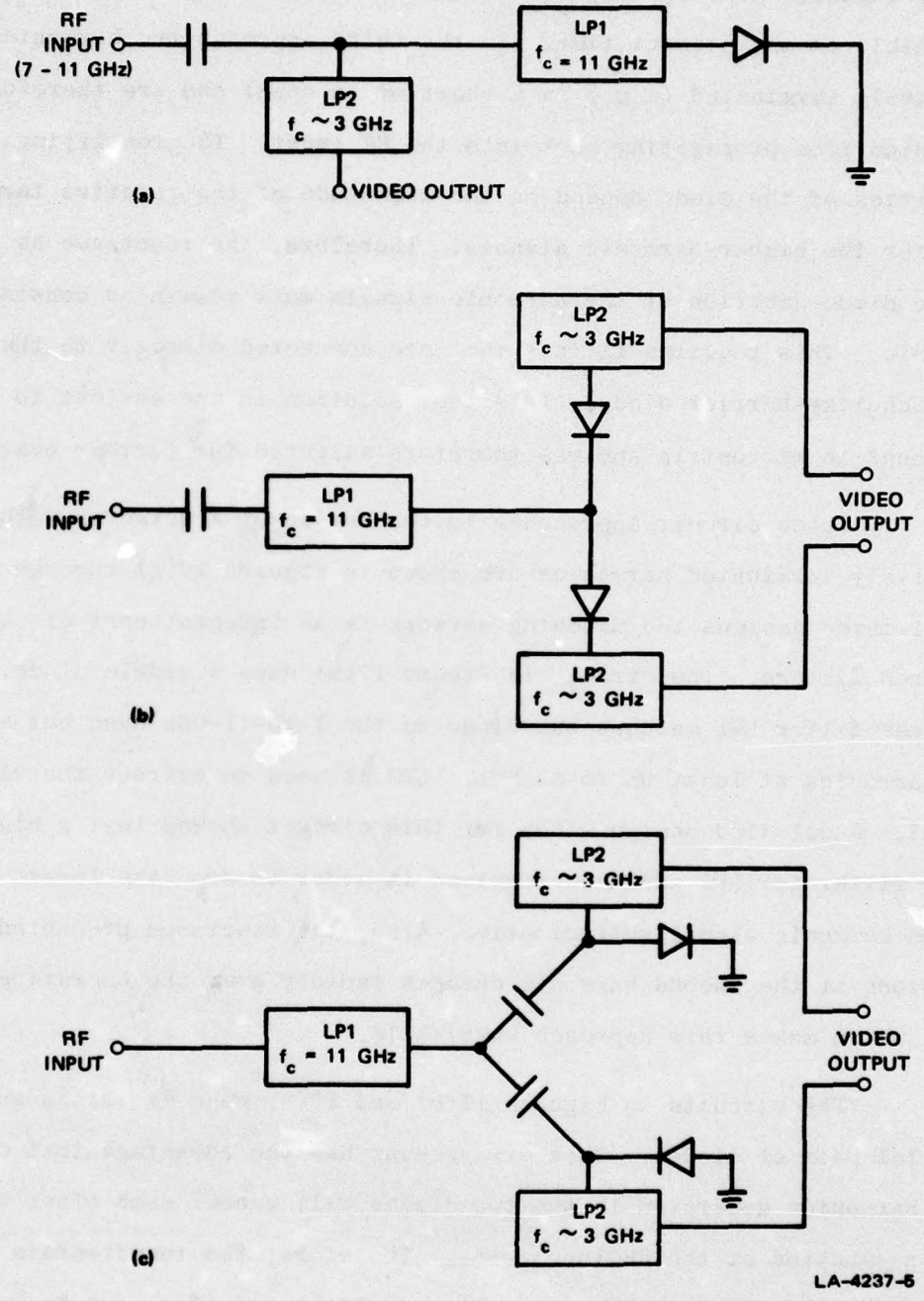

FIGURE 17 THREE DETECTOR CIRCUITS WITH REACTIVELY TERMINATED HARMONICS

7 GHz to at least 33 GHz, which is not easily achievable. In the circuit of Figure 17(c), LP2 has to present an open circuit to the diode at the fundamental and the third harmonic. The input impedance at the second harmonic appears relatively unimportant, because the filter is connected to a point that is almost a virtual ground. However, interactions between LP1 and LP2 at the third harmonic frequencies were partially responsible for the harmonic absorption problem observed with the first detector design (incorporated into Model 1 discriminators). Preliminary design work indicated the superiority of the circuit of Figure 17(c), and that circuit was therefore the only one pursued any further.

2. Development of Detector and Multiplexer

A silicon Schottky-barrier diode in beam-lead form from Hewlett-Packard (HP 5082-2769) was selected for use in the discriminator. Each diode is biased to have a junction resistance of 60 ohms under an incident RF power of -10 dBm. At this bias level the diode has the following electrical parameters:

Junction capacitance, C_j	0.14 pF
Series resistance, R_s	6 ohms
Series inductance, L_s	0.1 nH
Package capacitance, C_p	0.02 pF .

An initial circuit topology and associated element values were determined, based on existing filter designs and corresponding element values. This initial design was later improved by computer optimization. This technique has the important advantage that realistic upper and lower limits can be imposed on the variable circuit elements. Therefore, the practical realizability of the circuit elements is guaranteed. The optimization routine minimized the VSWR in the passband from 7 to 11 GHz and simultaneously achieved a high rejection in the band from 21 to

33 GHz. Figure 18 shows the equivalent circuit of the first detector with the final element values as obtained from the computer optimization. This result was obtained after three iterations of computer optimization and measurement of an actual microstrip realization of the circuit. A photograph of the actual microstrip circuit can be found as part of the photograph of the overall discriminator circuits [Models 1 and 1(a) in Figures 6 and 8, respectively]. The theoretical input VSWR and attenuation of this detector are shown in Figure 19(a). The maximum VSWR in the 7-to-11 GHz range does not exceed 1.07. In the stopband the attenuation increases gradually to very high values. However, low attenuations occur at 26.5 and 31.5 GHz. These two frequencies coincide with the third harmonics of those frequencies, for which the discriminator response exhibited strong irregularities. More insight into their origin is given by Figure 19(b), which depicts the reflection coefficient as seen from the junction resistance looking backward into the matching network. The second-harmonic termination varies over a 45° segment of the Smith chart, and is capacitive. The third-harmonic termination is also capacitive, but exhibits two resonances for which the junction resistance sees an almost perfect match. It is at those two frequencies that the third harmonics are terminated, and therefore half the power generated at the harmonics is dissipated outside the junction resistance and is no longer available for conversion to a dc signal. The source of both resonances is in the design of the matching and filter network. At the two resonant frequencies, R_j is matched into R_s. A purely lumped network would be devoid of resonances of the kind observed. The conditions for the resonances result entirely from the periodic response of the filter using distributed elements, in combination with the lumped impedance of the diode. The circuit exhibits two resonances because of interactions between LP1 and LP2, which are built of stubs with widely differing lengths. The problem was not discovered during the initial design phase,

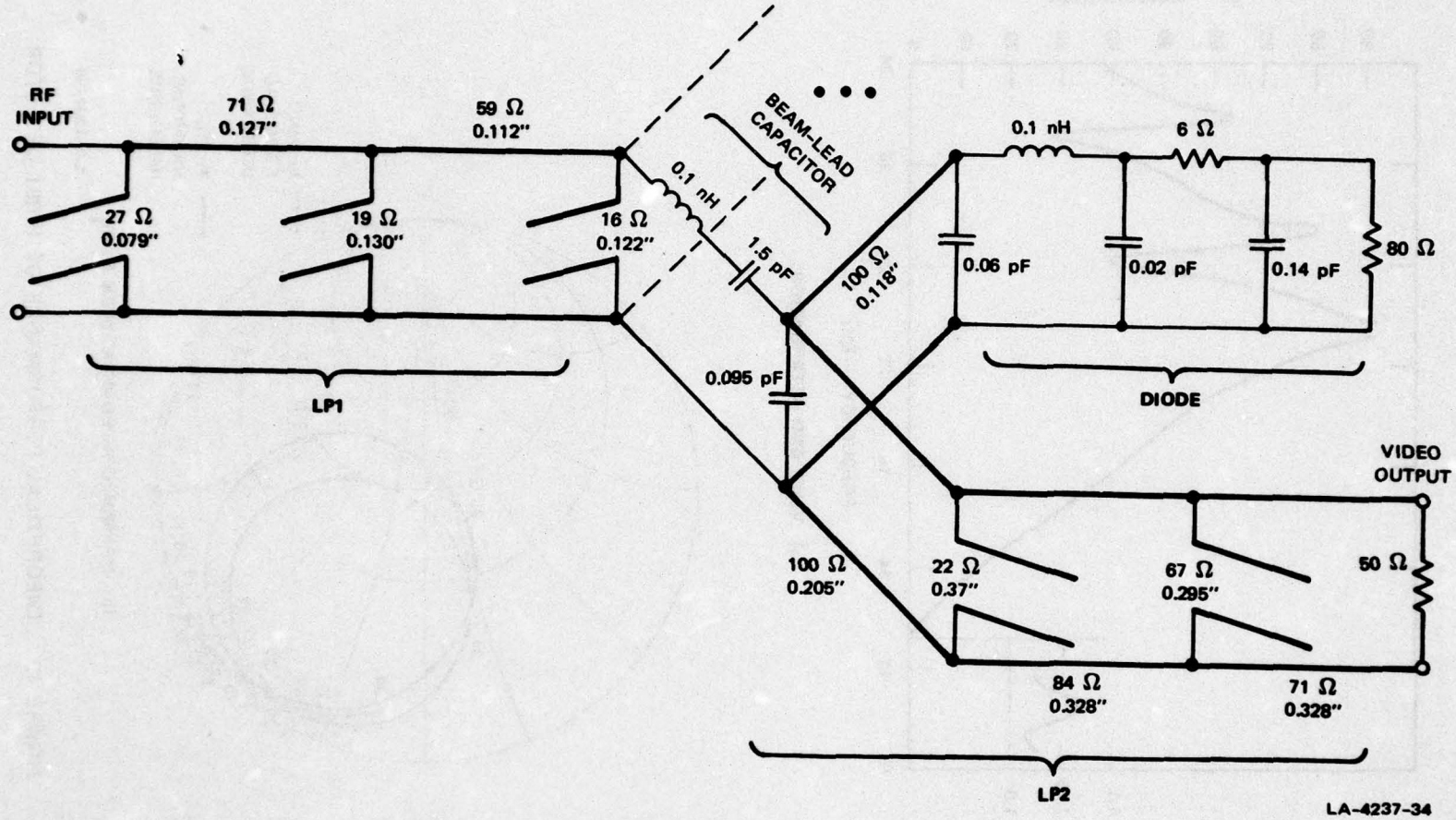

FIGURE 18 EQUIVALENT CIRCUIT OF FIRST DETECTOR

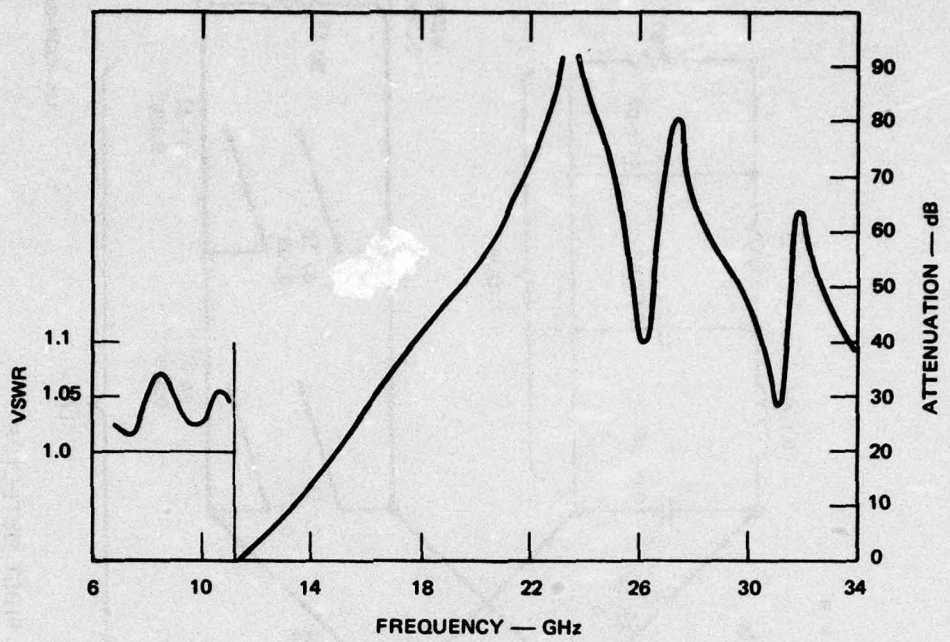

(a) VSWR AND ATTENUATION

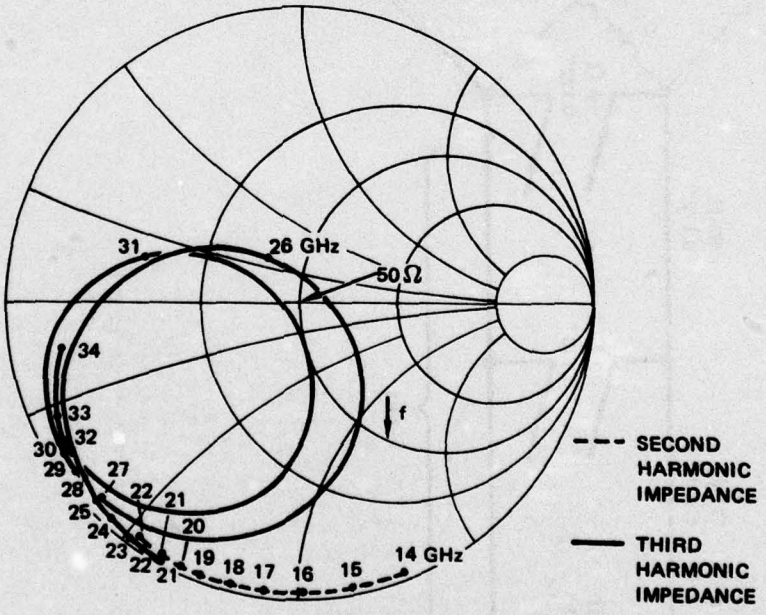

(b) HARMONIC IMPEDANCES SEEN BY R_j

LA-4237-35

FIGURE 19 THEORETICAL PERFORMANCE OF FIRST DETECTOR

because the number of frequency points used in the computer optimization was rather small, and the resonances were forced between sampled points. It was only much later that a recomputation of the loci in Figure 19 with finer frequency intervals revealed the presence of these resonances. An accurate measurement of the output voltage of the detector further corroborated the theory. (This measurement was made with the same computer-controlled system that was used to test the overall discriminator response.) The detector output voltage dropped abruptly by 3% near 10.5 GHz and somewhat less at 8.8 GHz. This voltage change compares with ripples of less than 1% caused by measurement inaccuracies and VSWR interactions.

The detector circuit was redesigned to eliminate the resonances at the third harmonic. Analysis disclosed that the potential for resonances exists as soon as the filter input impedance seen from the physical terminals of the diode exceeds approximately +j30 Ω. In the original detector design the interconnection of LP1 and LP2 was responsible for the lower resonance. The higher resonance was caused by LP1 itself, because the stub closest to the diode resonates at 24.2 GHz and renders the input impedance inductive above that frequency. The circuit shown in Figures 20 and 21 was designed to correct both these problems. This new circuit differs from the original circuit primarily in that the interconnection point of the two individual diodes has been moved toward the input of the detector, thereby making it possible to isolate LP2 from the diodes. At the same time, LP2 was simplified to a three-element filter. The new interconnection point also made it possible to split a large portion of LP1 and to build it separately for both diodes. This approach reduced the lengths of the stubs by approximately one-half,

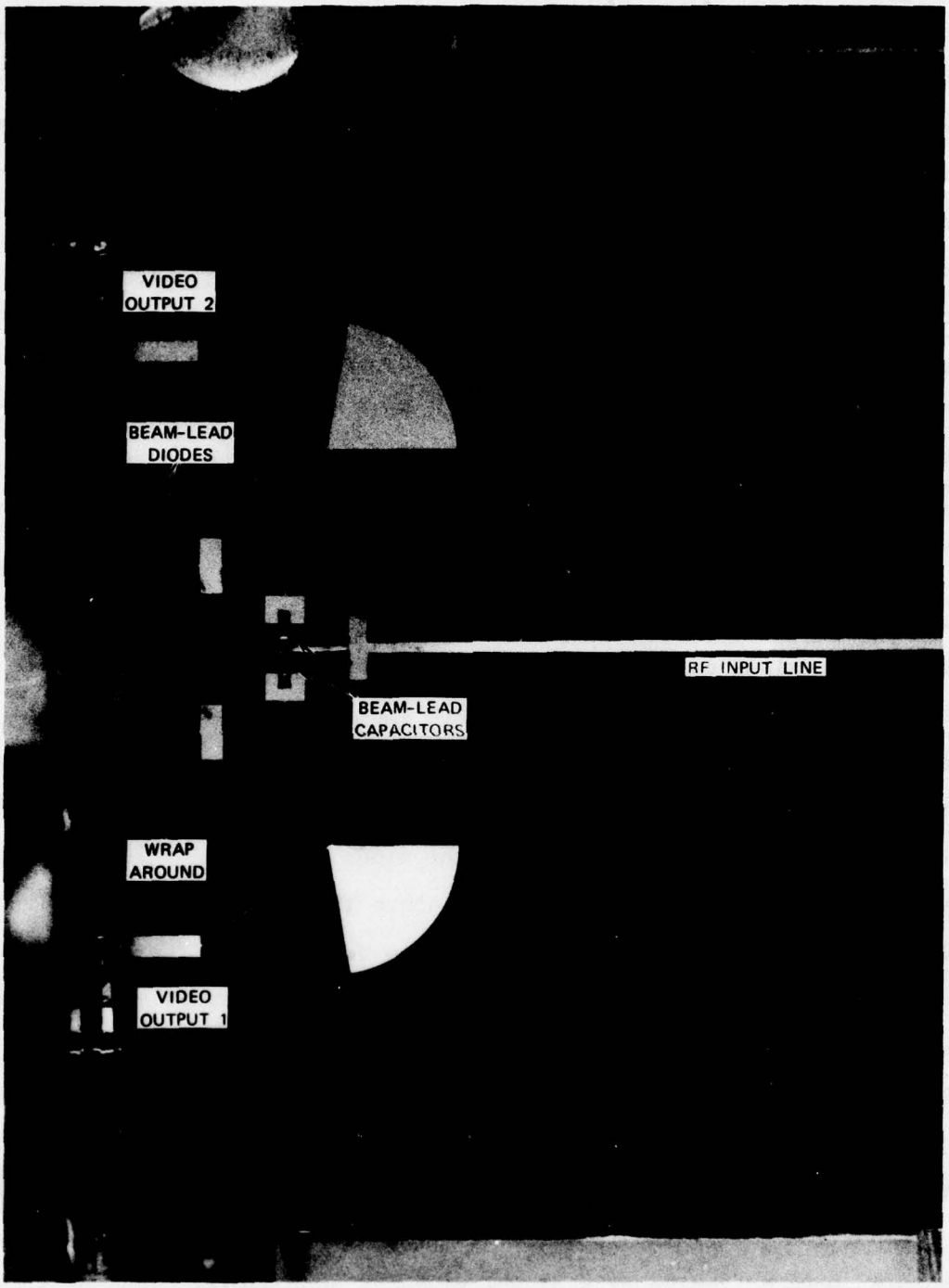

LA-4237-36

FIGURE 20 PHOTOGRAPH OF IMPROVED DETECTOR

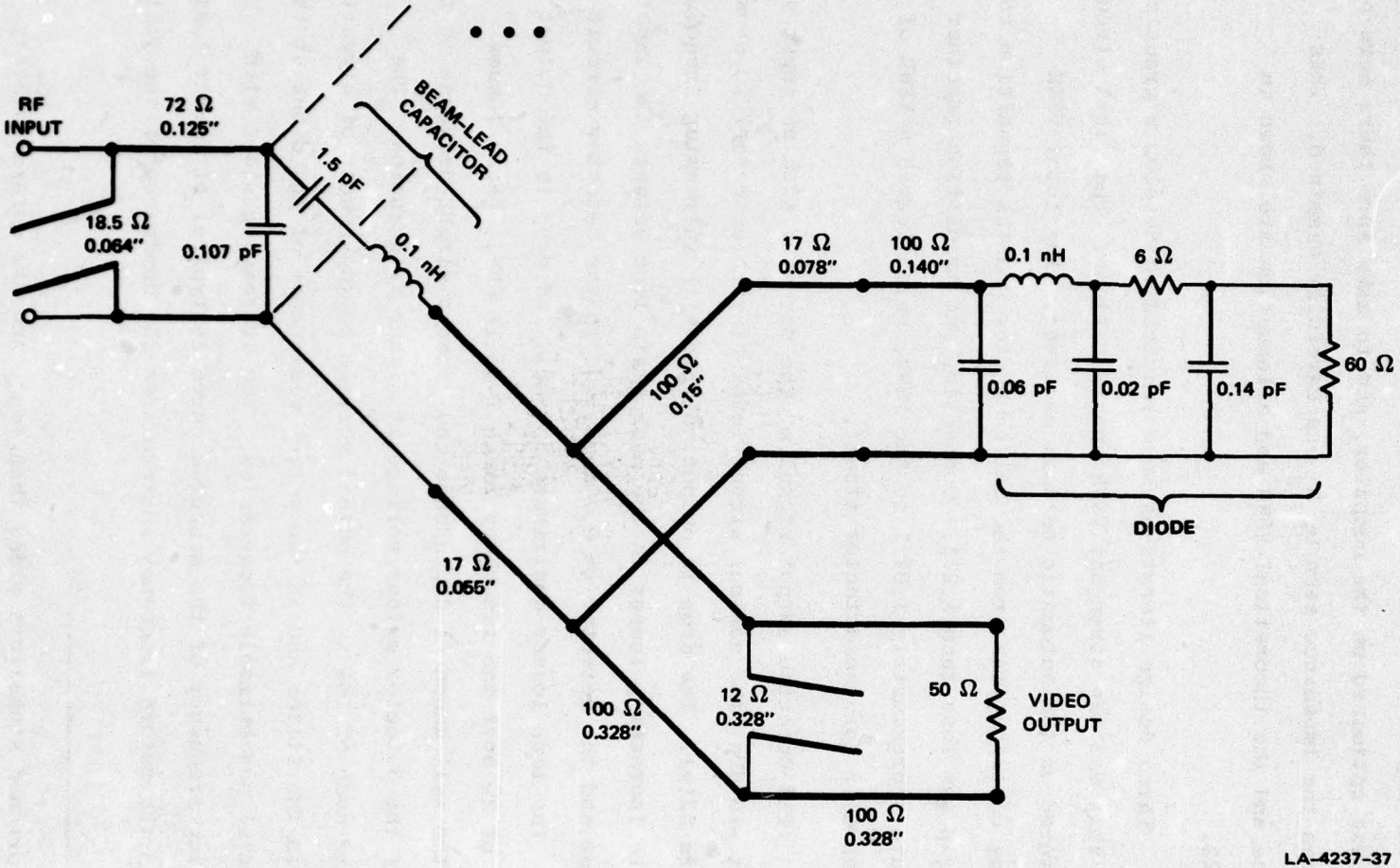

FIGURE 21 EQUIVALENT CIRCUIT OF IMPROVED DETECTOR

thereby raising their resonant frequencies beyond 33 GHz.* The new circuit was optimized on the computer, and to make sure there were no resonances the impedance seen by R_j was carefully examined. This impedance and the theoretical VSWR and attenuation are shown in Figure 22.

Three design iterations were required to develop a practical circuit that met the stringent VSWR specifications. The final circuit was measured on the automatic network analyzer. The total VSWR including contributions from the SMA connector and the transition to microstrip was less than 1.2:1. Connection and transition together contribute approximately 1.07:1 to the VSWR, which leaves a VSWR of less than 1.12 for the detector itself.

The detected output signal of the detector with an input power level of -10 dBm (the nominal signal level at each detector) is shown in Figure 23(a). The drop in output voltage with increasing frequency is due to increasing losses in the microstrip line between the input connector and the detector ($\approx$ 0.7 inch) and in the detector circuit itself. The line losses contribute an estimated drop in the output voltage of 2% over the frequency range 7 to 11 GHz. These losses follow the well known $\sqrt{f}$-dependence and cause a slight decrease in the slope of the detector output voltage at higher frequencies. The remaining drop of 16% in the output voltage is the result of circuit losses in the filter and in the series resistance of the diode at the fundamental and harmonic frequencies. The increasing slope with increasing frequency of the measured curve is typical of filter losses close to the cutoff frequency and confirms the dominance of the filter

---

*The shortened stubs were wider than long, and are more accurately represented by cascaded transmission-line sections.

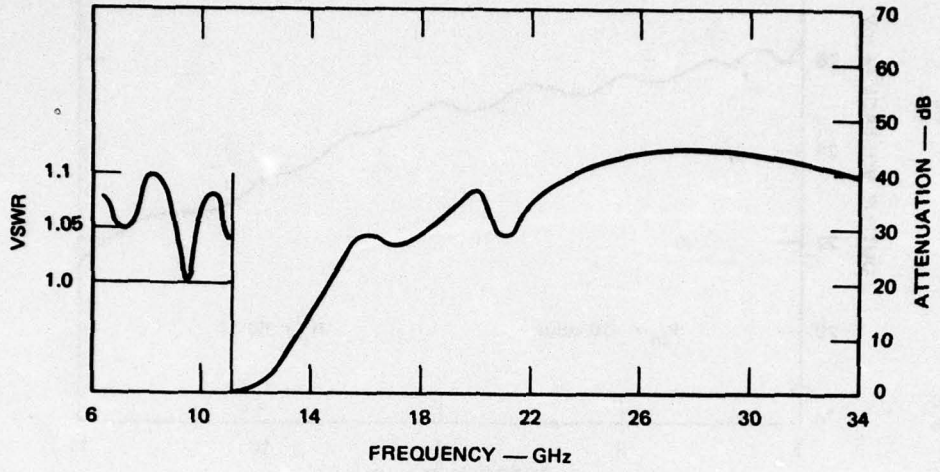

(a) VSWR AND ATTENUATION

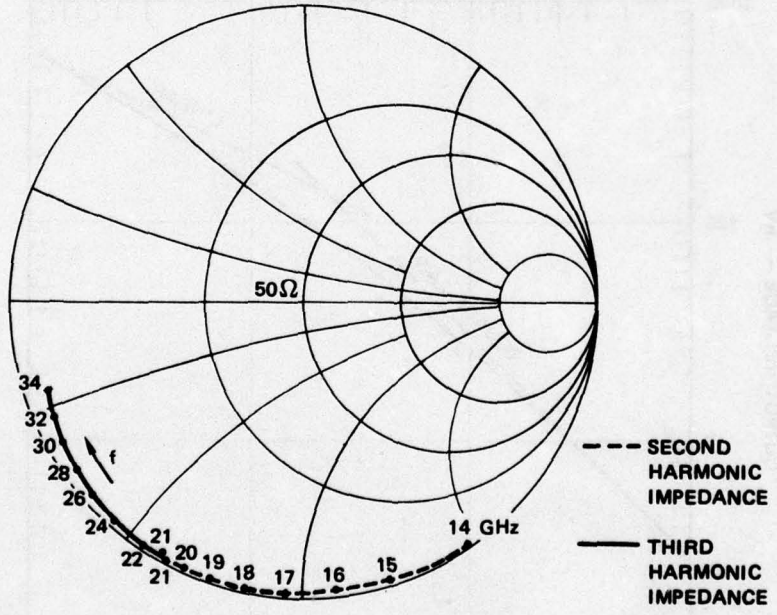

(b) HARMONIC IMPEDANCES SEEN BY R_j

LA-4237-38

FIGURE 22 THEORETICAL PERFORMANCE OF IMPROVED DETECTOR

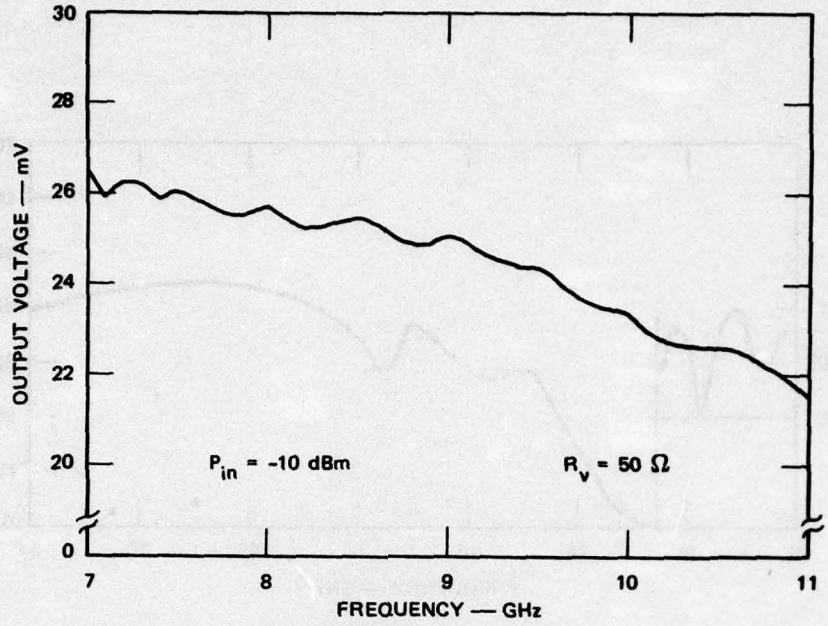

(a)

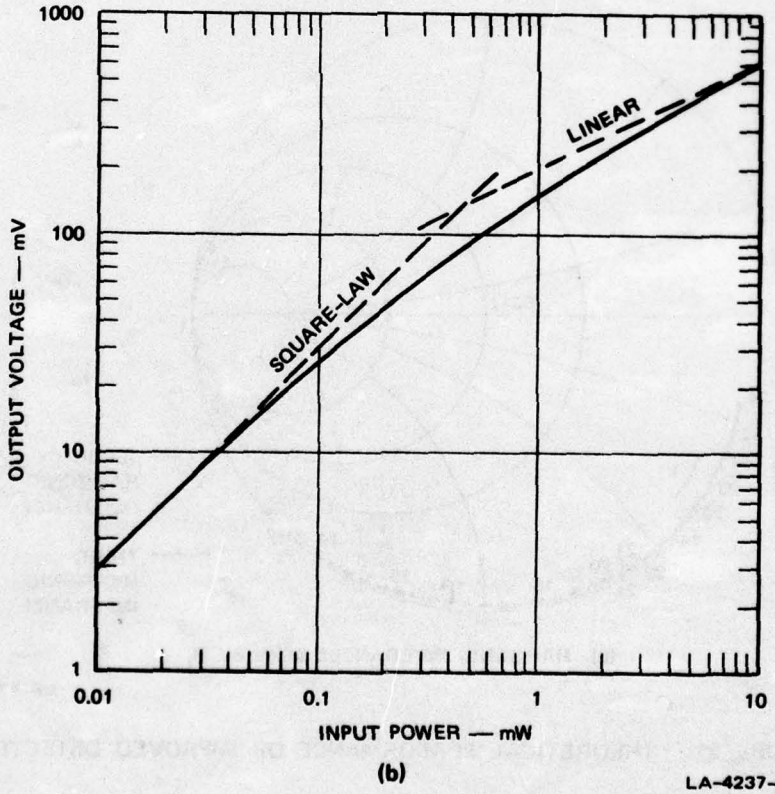

(b)

LA-4237-39

FIGURE 23 OUTPUT VOLTAGE AND TRANSFER CHARACTERISTIC OF IMPROVED DETECTOR

losses over the line losses. This sloped detector output voltage is the primary cause of the curved output characteristic of the uncompensated discriminator.

The output voltage versus input power for this detector is shown in Figure 23(b). The slopes for perfect square-law and linear operation are also indicated. At 0.1 mW input power, the transfer characteristic is in the transition region between the two regimes and can be characterized by Eq. (4) with $\alpha = 0.875$ and $\gamma = 187$ mV/mW. The video impedance of a single diode, R_v, was determined by measuring the output voltage for different video load impedances, R_L. A value of 50 ohms for R_v was found at the diode current that simultaneously gave the best RF match.

It was shown theoretically in Section III that tracking of the pair of detectors is the single most important requirement of the frequency discriminator. This tracking was studied by measuring two identical detectors fabricated on the same substrate. Tests were performed for two intermediate versions of detector Model 1. The complex reflection coefficients of both detectors were measured under identical conditions. The magnitude of the difference of the two reflection coefficients was found to be less than 0.048 at all frequencies, with an average value of 0.02 (i.e., $|\rho_R| \leq 0.024$).

The frequency-dependent tracking error is caused by the frequency-dependent power delivered to each detector and its effect on the detector input impedance. At the bandedges of 7 and 11 GHz the following maximum tracking errors were measured: $|\rho_F|_{max} \leq 0.058$ for a video load impedance $R_v = 200$ ohms, and $|\rho_F|_{max} \leq 0.024$ for $R_v = 50$ ohms. The lower video impedance significantly reduces the frequency-dependent tracking error.

No direct measurements of the harmonic signal level in the detector were made. However, to obtain an estimate of the filter rejection for the harmonic signals, RF signals in the bands from 14 to 22 GHz and 21 to 33 GHz were applied, and the filter attenuation was determined from the detected signal amplitude. These measurements were in good agreement with the theoretical attenuation shown in Figure 22(a).

C. Attenuator and Termination

1. Attenuator

The frequency-discriminator computer analysis showed that improved linearity can be obtained by incorporating 3-dB attenuators between the two couplers. Various lumped and distributed attenuators were evaluated and the circuit shown in Figure 24 was selected. Lumped attenuators in π or T-form exhibit wide bandwidth (down to dc) and excellent VSWR. In a microstrip circuit, the ground connections required for two of the three resistors in the π-circuit of Figure 24(a) are undesirable. Because of the high resistance values of the shunt resistors for a 3-dB attenuator, an open-circuited quarter-wave stub of a low characteristic impedance can be used as a good RF short over a restricted band of frequencies. Calculations for the circuit of Figure 24(b) indicate a maximum VSWR over the full 7-to-11-GHz band of 1.012. Because the desired attenuation is only 3 dB, the value of the series resistor and the value of the two shunt resistors differ by more than an order of magnitude. Thus, large differences are required in the aspect ratios of thin-film resistors of a fixed surface resistivity (e.g., 100 ohms per square). In particular, the series resistor would have a gap width of only 0.0017 inch for a 0.010-inch line and a surface resistivity of 100 ohms per square. By widening the linewidth, the gap for the series resistor can be enlarged proportionately as shown in

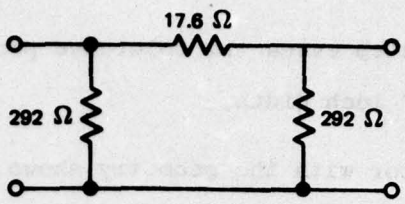

(a) MATCHED π-NETWORK 3-dB ATTENUATOR

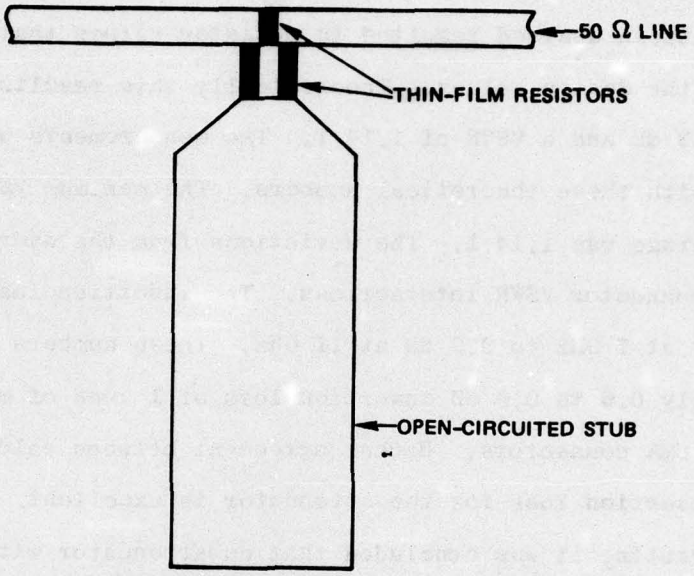

(b) MICROWAVE IMPLEMENTATION OF ATTENUATOR

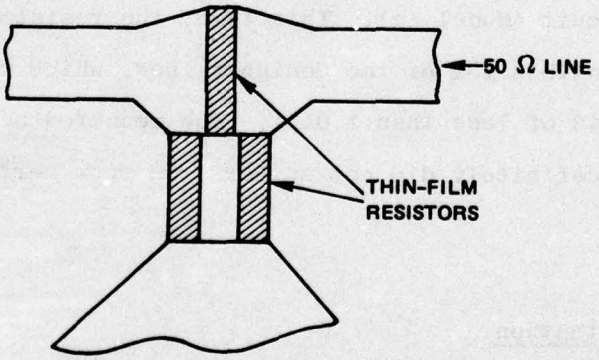

(c) MODIFIED GEOMETRY WITH WIDER SERIES-RESISTOR GAP

LA-4237-9

FIGURE 24 3-dB ATTENUATOR DESIGN

Figure 24(c). This step eases the tolerance problem existing in etching narrow gaps of 0.0017 inch width.

An attenuator with the geometry shown in Figures 24(b) and 24(c) was fabricated and tested. The actual circuit can be found in the photograph of the discriminator substrate, Model 1a, Figure 8. Minor deviations in the actual etched pattern of the test attenuator from the pattern desired resulted in resistor values that were 20% lower than the design values. Theoretically this results in an attenuation of 3.13 dB and a VSWR of 1.14:1. The measurements were in close agreement with these theoretical numbers. The maximum VSWR was 1.3:1 and the average was 1.14:1. The deviations from the average VSWR are caused by connector VSWR interactions. The insertion loss increased from 3.7 dB at 7 GHz to 3.9 dB at 11 GHz. These numbers include approximately 0.6 to 0.8 dB insertion loss of 1 inch of microstrip line and of two SMA connectors. Hence, agreement between calculated and measured insertion loss for the attenuator is excellent. Based on these measured results, it was concluded that an attenuator with the proper resistor values would have a very good VSWR and the proper insertion loss. Subsequently two of these attenuators were included in a discriminator circuit (Model 1a). This time, the resistor values were maintained to within ±3% of the design values, which resulted in a theoretical VSWR of less than 1.01:1. The measured performance of that discriminator definitely did not suffer from poor performance of the attenuators.

2. Termination

The isolated port of the first 3-dB hybrid has to be terminated in a matched load. For this termination a 50-ohm thin-film resistor was selected that is connected to ground with a wrap around

the edge. A model termination was built 10 times larger in size and optimized for best VSWR in the band of interest using a small capacitive island at the input of the termination to compensate for the inductance of the wrap-around. A VSWR of better than 1.1:1 was obtained in the model experiment. Measurements of an actual-size termination gave equally good results. The dc resistance of the tested termination was 48.4 ohms and the VSWR in the band from 7 to 11 GHz did not exceed 1.1:1. This value again includes residual connector contributions, indicating that the termination itself has an even better VSWR.

A chip resistor instead of a thin-film resistor was used in the first discriminator (Figure 6). This termination was also tested individually and found to have a VSWR not exceeding 1.2:1. Because of the importance of a good termination of the first 3-dB hybrid, thin-film terminations were used on most discriminator substrates fabricated after the first one.

D. Shaping Network

The function of the shaping network is to provide a frequency-dependent attenuation that is complementary to the internal loss of the discriminator. Numerous circuits, commonly known under the name gain equalizer, exist that provide-frequency dependent attenuation and have a low input VSWR. Two typical circuits suitable for MIC realization are shown in Figure 25. The circuit in Figure 25(a) is particularly convenient for MIC, because no ground connections are required. The loss-determining elements are R and Z_3. Maximum loss occurs when ℓ_3 is $\lambda_g/4$ long, and again at $3\lambda_g/4$, $5\lambda_g/4$ etc., as shown in Figure 25(c). The loss is a minimum when ℓ_3 is a multiple of $\lambda_g/2$. Two identical stubs, spaced approximately $\lambda_g/4$ at the center of the band of interest, improve the input VSWR of the circuit. Further improvements are possible by placing additional quarter-wave transformers at the input and output

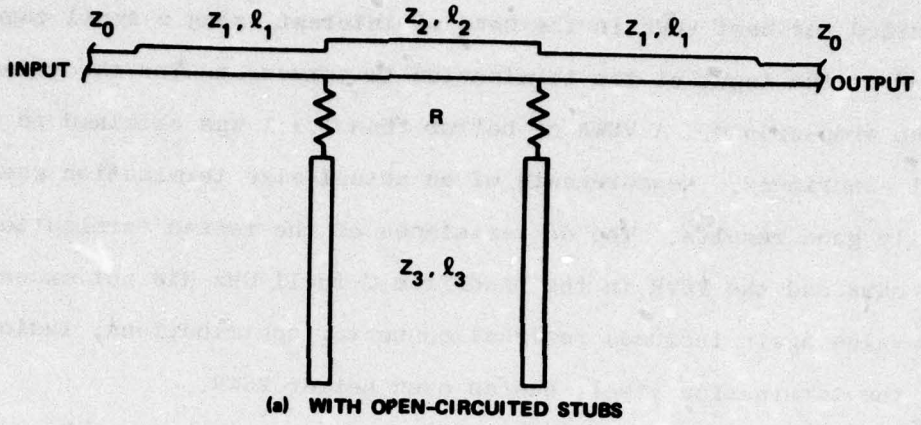

(a) WITH OPEN-CIRCUITED STUBS

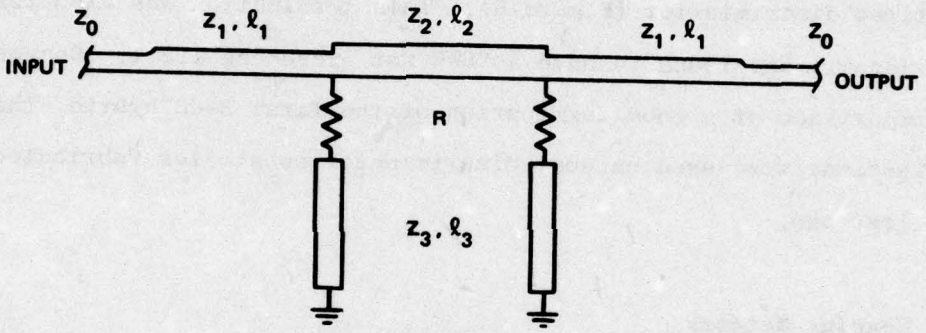

(b) WITH SHORT-CIRCUITED STUBS

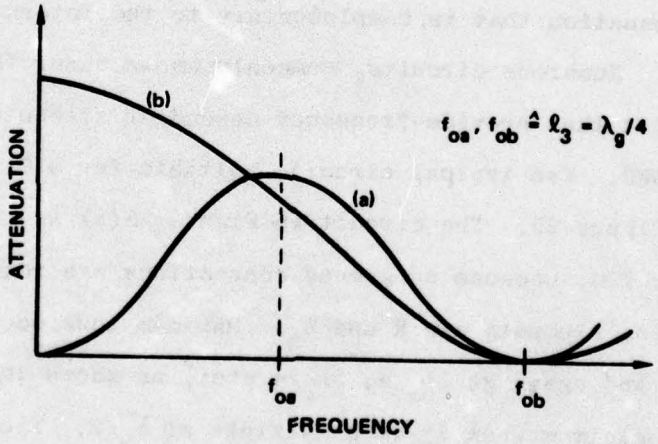

(c) FREQUENCY RESPONSE

LA-4237-40

FIGURE 25 TWO SHAPING-NETWORK TOPOLOGIES

(Z_1, ℓ_1). For application in the frequency discriminator, ℓ_3 would be selected to be $\lambda_g/4$ at 6 GHz. Minimum loss would then occur again at 12 GHz. The linearity of this circuit over the 7-to-11-GHz band proved insufficient because maximum and minimum attenuation occur too close to the bandedges. The circuit of Figure 25(b) has better linearity because of its reduced periodicity. The stub length ℓ_3 should be selected to be $\lambda_g/4$ at 12 GHz or higher. A further advantage of this circuit becomes evident when one tries to find element values for a gain slope of 2 dB from 7 to 11 GHz. For this gain slope the circuit with short-circuited stubs yields impedances that vary over a 1:3 range, whereas the other circuit requires twice that impedance range. A disadvantage of the former circuit is the requirement for short-circuited stubs. However, if the shorts are placed at the edge of a substrate they do not represent any substantial difficulty. For these reasons the circuit of Figure 25(b) was selected for the shaping network.

To verify the concept of the shaping network, the typical discriminator response of Model 1, Figure 7, was taken and a shaping network was designed that would have compensated the losses of that discriminator. A circuit employing thin-film resistors was built on a separate substrate (see Figure 26). Tests showed excellent agreement between theory and experiment, as can be seen from Figure 27. The theoretical response was calculated under the assumption of a constant $Q_u = 150$ for all transmission lines of the shaping network. This response differs significantly from the measured one, because the frequency dependence of Q_u and losses of the additional 50-ohm-line sections at both ends of the network are not included. When they are included, the agreement becomes excellent.

Following the successful test of the trial shaping network, a network of identical topology was designed to fit a discriminator substrate

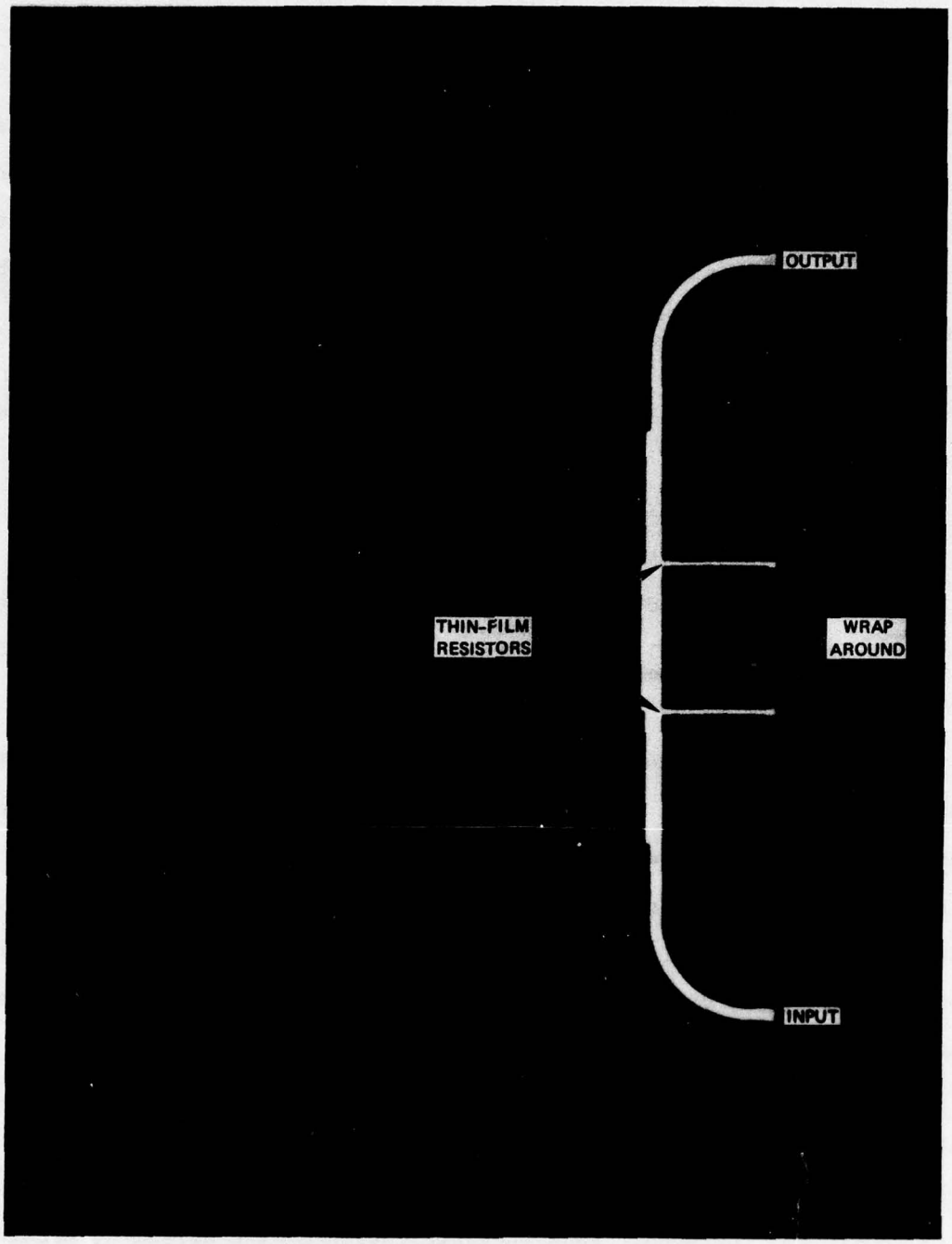

LA-4237-41

FIGURE 26 PHOTOGRAPH OF TRIAL SHAPING NETWORK

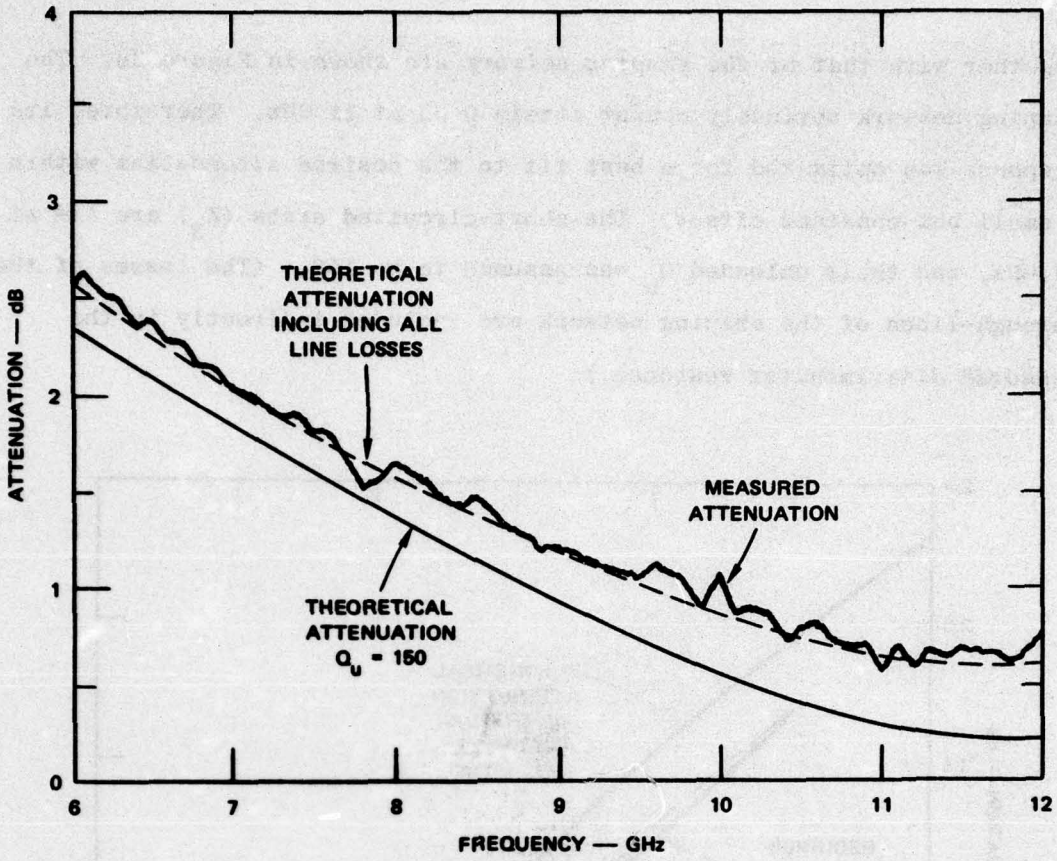

SHAPING NETWORK OF FIGURE 25(b)

Z_1 = 41 Ω	ℓ_1 = 0.31"
Z_2 = 36 Ω	ℓ_2 = 0.36"
Z_3 = 75 Ω	ℓ_3 = 0.236"
R = 80 Ω	

LA-4237-42

FIGURE 27 THEORETICAL AND EXPERIMENTAL RESPONSE OF TRIAL SHAPING NETWORK

Model 1 that had been fabricated for the planned linearized discriminator. In order to make an accurate account of the line losses of the equalizer, a substrate with a 50-ohm microstrip line of the same length as that of the future equalizer was placed at the input to the discriminator substrate. Then the discriminator response was measured and the required gain compensation determined. This was done by use of the output voltage-to-input-power relationship for the detectors--Eq. (4)--including the previously measured exponent $\alpha = 0.875$. The required attenuation

together with that of the shaping network are shown in Figure 28. The shaping network obviously cannot attain 0 dB at 11 GHz. Therefore, its response was optimized for a best fit to the desired attenuation within a small but constant offset. The short-circuited stubs (Z_3) are $\lambda/4$ at 12 GHz, and their unloaded Q_u was assumed to be 150. (The losses of the through-lines of the shaping network are included indirectly in the measured discriminator response.)

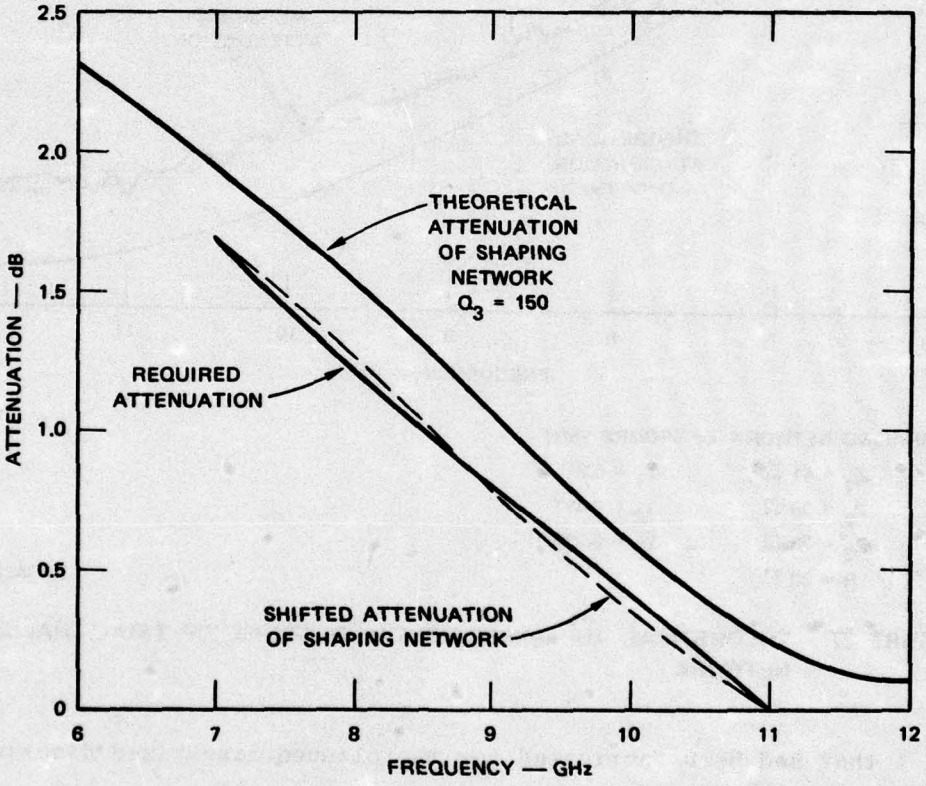

SHAPING NETWORK OF FIGURE 25(b)

Z_1 = 40.8 Ω	ℓ_1 = 0.31"
Z_2 = 36 Ω	ℓ_2 = 0.36"
Z_3 = 65 Ω	ℓ_3 = 0.236"
R = 95 Ω	

LA-4237-43

FIGURE 28 APPROXIMATION OF REQUIRED ATTENUATION WITH SHAPING NETWORK

This shaping network was not tested independently. Rather, it was directly integrated with the discriminator and the output was adjusted for best linearity. The shaping network fully proved its effectiveness. However, the overall discriminator response still showed the irregularities at 8.8 and 10.7 GHz due to the absorption of the harmonics. The attenuation characteristic of the shaping network needed to linearize the response of the improved discriminator (Model 2) was determined, and was found to be close to the attenuation characteristic of the original discriminator. Therefore the new discriminator was tested with the old shaping network, and the results are presented in Figure 13. Apparently, the tolerance range of the attenuation slope of the shaping network is fairly large--of the order of ±0.3 dB at 7 GHz. These results demonstrate that it is possible to build a single equalizer to match a given discriminator design. Minor differences from unit to unit can be compensated for by adjusting the detector-diode bias currents.

E. Video Amplifier

The video amplifier performs five functions:

(1) It sums the output voltages of the four detector diodes. The video output voltages of two diodes are positive and the output voltages of the other two are negative. Hence, a differential amplifier is required to sum all output voltages.

(2) It provides the bias current for the detector diodes.

(3) It provides a dc-offset adjustment for shifting the discriminator output to all-positive voltages.

(4) It provides sufficient gain to reduce the gain and noise-figure requirements of the following amplifier stages.

(5) It performs the important function of decoupling the detector diodes from the rest of the video chain.

Because the discriminator output must be accurate on a pulse-to-pulse

basis, independent of pulsewidth and pulse repetition rate, a dc-coupled amplifier is necessary. The total response time--i.e., delay time, rise time, and settling time to 1% of the final value of the video amplifier--must not exceed 25 ns. A differential operational amplifier is capable of performing the five functions within the desired response time.

In the design of the amplifier, emphasis was placed on meeting the required response time while maintaining a low noise figure and high gain. Early in the program, during the attempt to obtain sufficient bandwidth, the noise properties of the amplifier were overlooked. This resulted in an amplifier with an excessive noise figure, and a redesign was required. The following description covers some of the difficulties experienced and the design of the final amplifier.

The discriminator output SNR is a function of the RF input power, the detector sensitivity, and the noise figure of the amplifier. The RF input power was fixed at -6 dBm by the output of the tunnel-diode limiter. The sensitivity of the detectors was effectively set by the comparatively high bias current of 0.5 mA. This current was required in order to maintain a low RF VSWR for the detectors. Thus, the only way left to improve the output SNR was to use a video amplifier with a low noise figure. This fact can be further appreciated by considering the equation for the nominal detectable signal NDS, (SNR = 1), as given by Uhlir:[6]

$$NDS = \frac{2}{\gamma}\sqrt{kTR_v\left[Bt_w + \frac{T_o}{T}(F_v - 1)B + f_x \ln\frac{f_h}{f_\ell}\right]} \qquad (14)$$

where

γ = Voltage sensitivity of the detector

k = Boltzmann constant

T = Absolute temperature of the diode

T_o = 295 K

B = Bandwidth of the video amplifier

t_w = White-noise ratio of the detector (≈ 1)

F_v = Noise figure of the video amplifier

f_x = Flicker-noise corner frequency (at f_x, flicker noise equals white noise)

f_h = Upper video bandedge frequency

f_ℓ = Lower video bandedge frequency.

The quantities R_v, γ, and f_x are all functions of the bias current. To a first approximation the following relationships hold

$$R_v = \frac{kT}{qI_o} \tag{15}$$

$$\gamma = \frac{1}{2I_o} \tag{16}$$

$$f_x = f_x' I_o \tag{17}$$

where

q = Electron charge

I_o = Bias current

f_x' = Normalized corner frequency.

Typical values for f_x' for a Schottky barrier diode are 100 kHz/mA. The wide bandwidth of the video amplifier for the discriminator (f_h = 100 MHz, f_ℓ = 1 Hz assumed) makes the flicker-noise contribution in Eq. (14) insignificant; it can therefore be neglected. Inserting Eq. (15)

through (17) into Eq. (14) yields:

$$NDS = 4kT\sqrt{\frac{I_o}{q} B\left[t_w + \frac{T_o}{T}(F_v - 1)\right]} \quad . \qquad (18)$$

From Eq. (18) it is evident that the nominal detected signal is proportional to $\sqrt{I_o}$ (i.e., the detector loses sensitivity with increasing current). However, Eq. (18) is based on the assumption that there are no mismatch losses on the RF side. In general, it is difficult to match the diode for very low bias currents, particularly over large bandwidths. For very low bias currents the mismatch losses increase inversely proportional to $\sqrt{I_o}$, thus canceling the advantage of a low bias current indicated by Eq. (18). Overall, the NDS is relatively independent of bias current, at least for detectors with a wide video bandwidth where flicker noise is insignificant. The video-amplifier noise can easily be the dominant noise contributor in a detector, as seen from Eq. (18). Unfortunately, operational amplifiers tend to be noisier than ac-coupled amplifiers. This stems primarily from the fact that the amplifier itself has to be optimized for high gain and speed rather than low noise figure. Proper selection of the input resistors can be used to optimize the noise figure of a given operational amplifier. However, other design constraints limit possible improvements.

Figure 29 shows the basic schematic of the differential amplifier including the detector diodes used in this program. The output voltages of the four diodes are connected to the positive and negative inputs of the amplifier according to their polarity of the useful signal. Each pair of diodes connected to the same amplifier input uses opposite bias voltages, thus canceling any bias voltage offset. The gain of the amplifier is determined by R_F/R_1, and $R_E = R_F$ is required for equal gain from each diode input. The purpose of resistors R_2 is to lower the input

impedance of the amplifier without having to change R_1. These resistors lower the sensitivity of the system, but help improve the linearity of the discriminator and the rise time, as will be explained in more detail later. The basic differential amplifier scheme of Figure 29 was realized using three different operational amplifiers.

Initially, a circuit using a Burr-Brown Model 3400A amplifier was designed for unity gain and 70-MHz bandwidth. The amplifier turned out to be unsuitable, because internal characteristics limited the 3-dB bandwidth to less than 10 MHz. A second amplifier purchased from M.S. Kennedy

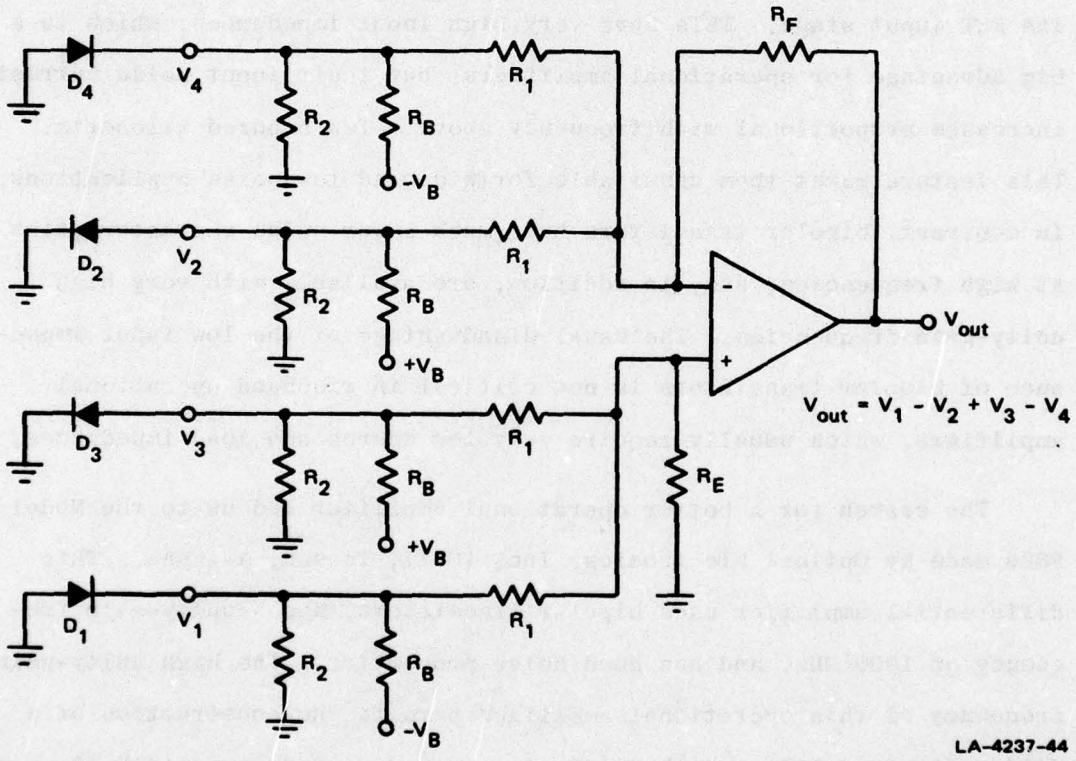

FIGURE 29 SIMPLIFIED CIRCUIT DIAGRAM OF THE DIFFERENTIAL VIDEO AMPLIFIER

Corporation (Model 850) provided unity gain and a -3 dB bandwidth of 45 MHz. Strong ringing limited the settling time to 50 ns, but the major drawback of this amplifier was its excessively high noise figure. Measurements showed a noise figure of 41.7 dB at 30 MHz, which increased with frequency until the gain rolloff eventually reduced the noise output power. It was estimated that the high output noise voltage of this amplifier could produce a high random error in the frequency readout of the discriminator of about ±250 MHz maximum. The exact error would be a function of the processing following the discriminator.

The high noise figure of the M.S. Kennedy amplifier is caused by its FET input stage. FETs have very high input impedances, which is a big advantage for operational amplifiers, but their input noise current increases proportional with frequency above a few hundred kilohertz. This feature makes them unsuitable for wideband low-noise applications. In contrast, bipolar transistors have much lower noise characteristics at high frequencies, and, in addition, are available with very high unity-gain frequencies. The usual disadvantage of the low input impedance of bipolar transistors is not critical in wideband operational amplifiers, which usually require very low source and load impedances.

The search for a better operational amplifier led us to the Model 9826 made by Optical Electronics, Inc. (OEI), Tucson, Arizona. This differential amplifier uses bipolar transistors, has a unity-gain frequency of 1000 MHz, and has good noise properties. The high unity-gain frequency of this operational amplifier permits the construction of a differential amplifier with 20 dB of gain and a -3 dB bandwidth close to 100 MHz.

For resistors, R_1, a value of 100 ohms was used because this low value gave better noise figures and helped to realize a small RC time constant formed by R_1 and the input capacitance of the operational

amplifier. A small time constant is desirable for high-frequency response. On the other hand, it was found that the frequency-dependent tracking error is minimized when the detector diodes see a 50-ohm load. However, lowering R_1 to 50 ohms resulted in increased ringing. Therefore the diode load impedance was adjusted to 50 ohms by selecting R_2 = 100 ohms. This resulted in an amplifier with good response time and optimum load impedance for the diodes at the expense of an increase in noise figure of approximately 3 dB.

The complete video amplifier schematic is shown in Figure 30. In comparison with Figure 29, the complete circuit has the added features of stabilization networks for the diode bias voltages (R13, R14, C1, C2, D1, and D2), potentiometers for the diode bias currents (R8 through R11), and a circuit for adjusting the output offset voltage (R15 through R19, C5, and C6). The voltage gain of the operational amplifier alone is 15 (23 dB). This gain is reduced to 20 dB by R25 at the output when operating into a 91-ohm load. The resistor R25 serves primarily as an isolating resistor. It decouples high-capacitance loads, which could cause instabilities, from the output terminal of the operational amplifier. In addition, R25 provides a fair match at the amplifier output.

Figure 31 shows the pulse response of the final amplifier. The delay time of the amplifier is 4 ns, and the rise time from 10% to 90% is 8 ns (the input pulse has 3 ns rise time). Total response time was measured with a circuit that permits displaying the difference between the input pulse and the output pulse, taking into account the gain of the amplifier. This difference is displayed in the lowest trace in Figure 31. Overall response time (1% settling) is estimated to be 25 ns. An accurate determination is difficult because of the imperfect input pulse. The measured time response is in good agreement with the measured frequency response. The amplifier shows a very flat response to

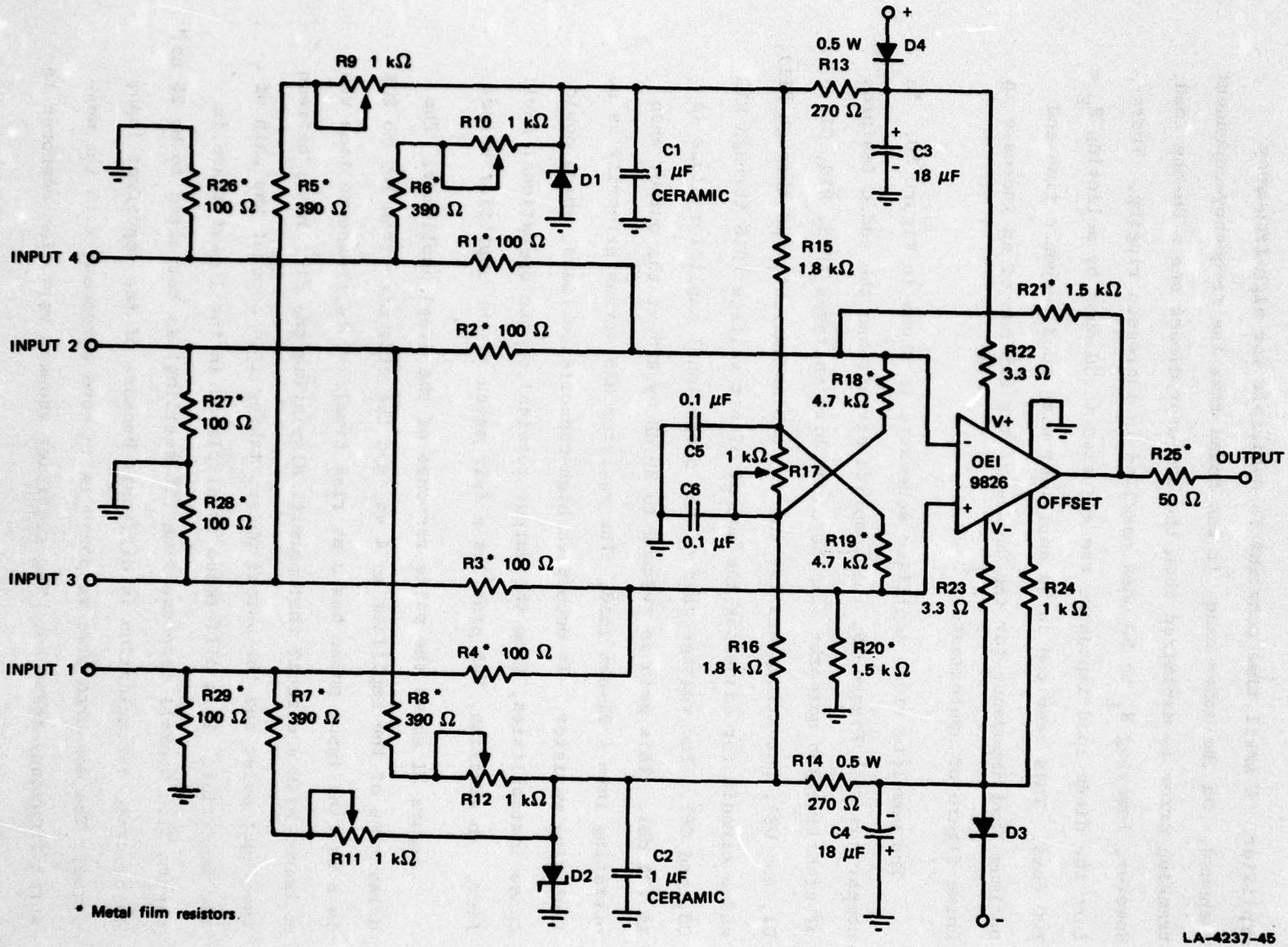

FIGURE 30 SCHEMATIC OF FINAL DIFFERENTIAL VIDEO AMPLIFIER

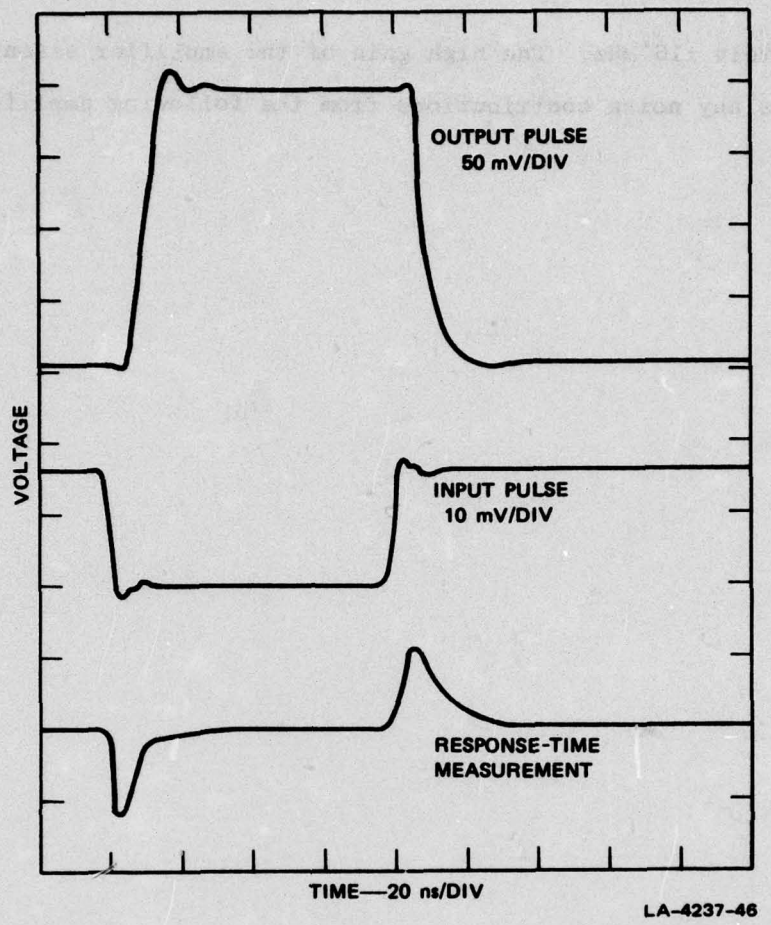

FIGURE 31 PULSE RESPONSE OF DIFFERENTIAL VIDEO AMPLIFIER

30 MHz, and then drops monotonically. The -3 dB point lies at 55 MHz, and the -10 dB point at 100 MHz. The rolloff has a slope of 8 dB per octave, which is slightly more than that of a single RC element. The noise figure of the amplifier was measured by comparing the output noise power of the amplifier in a 1-MHz band with that of an amplifier with a known noise figure (standard noise-figure meters could not be used because of the high noise figures of the amplifiers). The noise figure at 30 MHz is 17.5 dB. The measured peak-to-peak noise voltage referenced back to the input of the amplifier is 200 μV (measurement bandwidth 150 MHz). This corresponds to a worst-case frequency error of

approximately ±16 MHz. The high gain of the amplifier essentially eliminates any noise contributions from the following amplifier stage.

VI DISCRIMINATOR MEASUREMENT TECHNIQUE

A. Background

Measuring the static performance of a discriminator requires two instruments: a signal source with a very accurate frequency and power setting (e.g., a source followed by a perfect limiter), and a precision voltmeter. While it is easy to find an accurate voltmeter, it is extremely difficult to build or simulate a perfect limiter. Actually, each discriminator needs to be operated with a limiter, and therefore it would be most meaningful to test the combination limiter/discriminator as a whole. Without a suitable limiter and in order to measure the accuracy of the discriminator alone, it was necessary to simulate a very good limiter. Initial static measurements were made point by point, by carefully calibrating the power and frequency of the RF source. The output voltage was measured with a digital voltmeter. This procedure was very tedious and not very accurate. Also thermal drift of the detector diodes and the amplifier over the measurement time of several hours led to additional errors, even though the discriminator is to a first approximation insensitive to temperature changes because of its balanced construction.

A measurement procedure that was both much faster and more accurate was required in order to make tuning of the discriminator response practical by adjusting the diode bias currents. The system described below uses an Automatic Network Analyzer (ANA) to automate the measurements and the processing of the data. This system proved very helpful in developing the high-linearity discriminators; in fact, without it, the achieved results probably would not have been possible.

B. Computer-Controlled Measurement System

The measurement system was built around SRI's Hewlett-Packard Automatic Network Analyzer Model 8542B. A block diagram of the discriminator measurement system is shown in Figure 32. The ANA was used principally to provide a computer-controlled, frequency-synthesized signal source. Because most of the standard ANA wiring was bypassed, the phase-lock loop to the harmonic frequency converter had to be completed outside the existing wiring of the ANA. The internal leveling circuit was also replaced with an external coupler and detector, which were located as close as possible to the discriminator input port in order to minimize power fluctuations. A computer-controlled SPDT switch was used to turn the RF power off and on. Following the switch is a 10-dB attenuator, which sets the power level at -6 dBm. This attenuator was selected to provide a VSWR $\leq$ 1.1:1 at its output port, labeled "S" for source, to the discriminator (see Figure 32). The output voltage of either the power meter or the discriminator is measured with a computer-controlled digital voltmeter.

The measurement procedure consists of a calibration phase and a measurement phase, as detailed in the flow diagram of Figure 33. The measurement frequencies, the nominal input power level, and other data are entered, and the calibration factors of the power meter are then entered for the discrete frequencies of interest. The calibration factor takes into account the efficiency of the sensor, the mismatch error between the "source" and the power sensor, and the insertion loss of the required adapters. The latter two factors were determined in preparation for the discriminator measurements, whereas the efficiency of the sensor was taken from the manufacturer's calibration data. The calibration phase consists in measuring the output power from the "source" S. These data are stored and later used to correct the discriminator measurements for the deviation in the actual available power from the

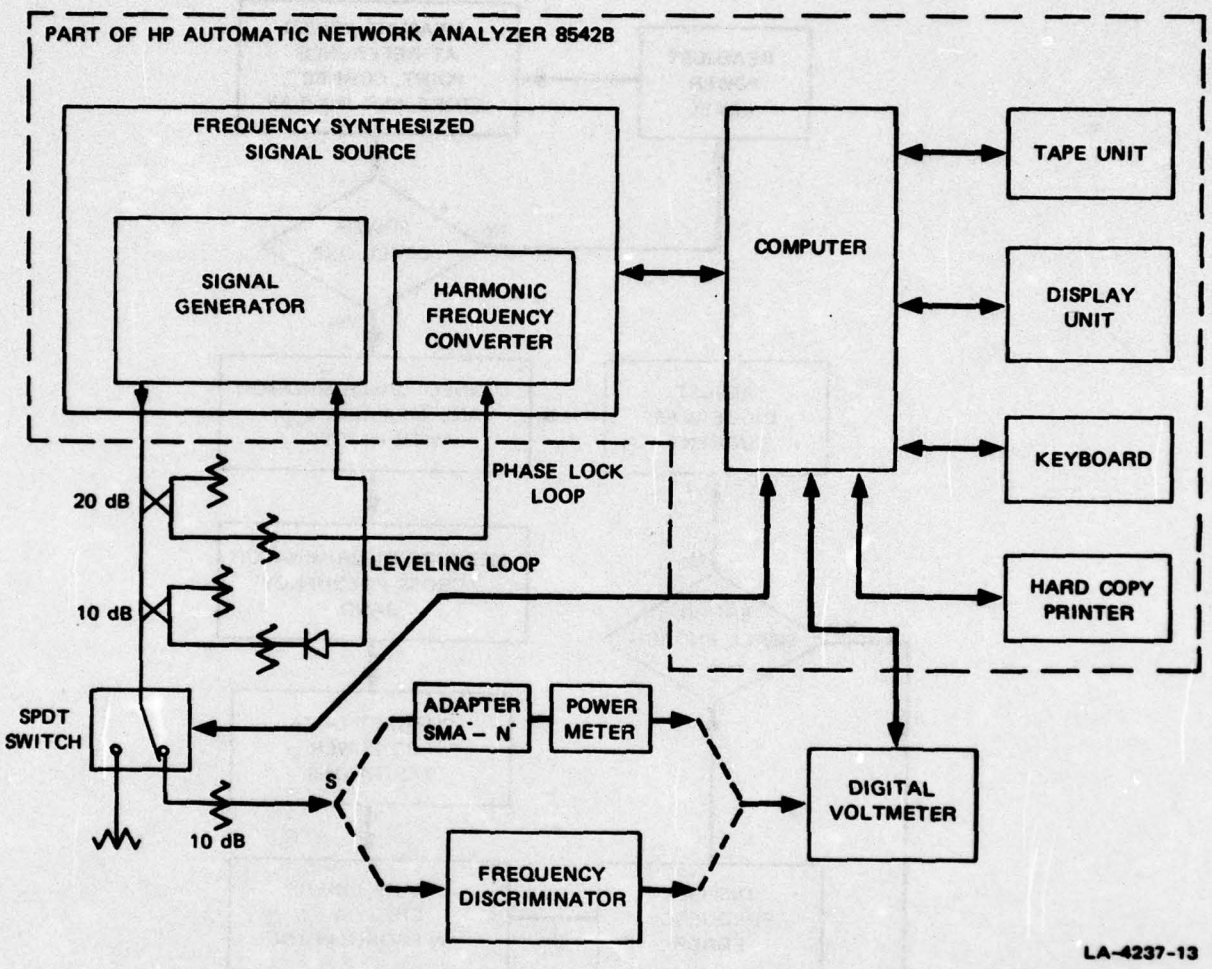

FIGURE 32 BLOCK DIAGRAM OF DISCRIMINATOR MEASUREMENT TEST SETUP

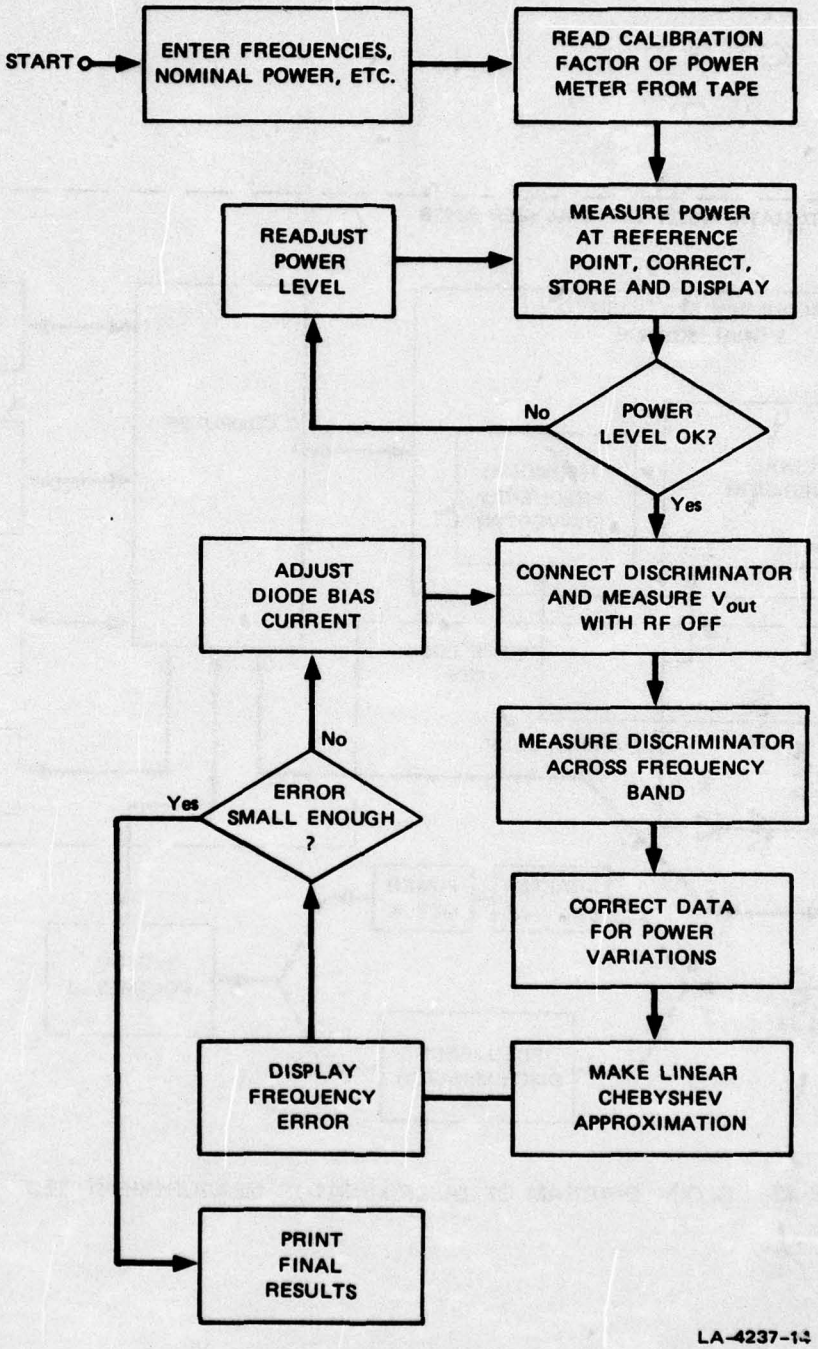

FIGURE 33 FLOW DIAGRAM OF DISCRIMINATOR MEASUREMENT PROGRAM

nominal power (in this case, -6 dBm). To minimize phase, the available power is adjusted as closely as possible to the nominal power level. Typically, a flatness of better than ±0.13 dB is achieved.

During the measurement phase the power meter is replaced by the frequency discriminator. The output voltage of the discriminator with the RF signal off, V_{vo}, is measured first. Then the output voltage with the RF on, V_{vi}, is measured at the discrete frequencies, f_i. The measured voltages are subsequently corrected for deviations from the nominal power level. Mathematically, these corrections are accomplished from a generalization of Eq. (6) or Eq. (7) as follows. For a detector with an arbitrary exponent α between 0.5 and 1, one can write

$$V_{out} = \gamma P_i^{\alpha} f(\theta_i) \quad , \quad f(\pi/2) = 0 \tag{19}$$

where P_i = Input power at f_i.

Power deviations from the nominal value, P_o, affect V_{out} proportional to $(P_i/P_o)^{\alpha}$. Due to the offset voltage added by the amplifier, the output voltage, V_{vi}, at midband is different than zero. Let V_{vi} at midband be denoted by V_{vm}. Hence, V_{out}, which requires corrections for power variations, is given by

$$V_{out} = V_{vi} - V_{vm} \quad . \tag{20}$$

Theoretically, V_{out} is zero at midband [see Eq. (19)] independent of P_i. This statement holds in particular for $P_i = 0$, and therefore V_{vm} has to be identical to the output voltage measured without RF power, V_{vo}. This conclusion must be questioned, because of the incomplete balance of diodes and of diode bias currents. However, tests with an actual discriminator showed that V_{vo} is an accurate representation of V_{vm}, even

though V_{vo} changes as the diode biases are adjusted. Hence, the corrected output voltage, V'_{vi}, is now determined by

$$V'_{vi} = \left(V_{vi} - V_{vo}\right)\left(P_i/P_o\right)^{\alpha} + V_{vo} \quad . \tag{21}$$

To facilitate adjustments of the bias currents for best linearity, both the output voltage and the frequency error versus frequency are displayed (see, e.g., Figure 7) on the graphics terminal of the ANA. Adjustment of bias currents and measurements are repeated until optimum linearity is obtained. If desired, the final results can be printed on a hard copier.

An error analysis was made to assess the accuracy of the measurement procedure. The frequency can be set to within 1 kHz by the ANA, and its error contribution is completely insignificant. The major source of error is the uncertainty in the power measurement during the calibration phase. An additional small error is contributed by the digital voltmeter used to measure the output voltage of the discriminator. The power measurement error is caused partially by errors in measuring the output voltages of the power meter. Because the power variations are very small, the power meter and the digital voltmeter both operate over only 5% of their full range and the relative error between maximum and minimum value is estimated to be less than 0.02%. An absolute error in this measurement is equivalent to a frequency-independent power error, which has no consequences for the linearity of the discriminator.

The more significant power measurement errors are due to uncertainties in the overall efficiency of the power-meter sensor. Three factors have been considered: mismatch losses between the "source" and the sensor, adapter losses, and the efficiency of the sensor itself. Mismatch errors were calculated from ANA measurements of the reflection

AD-A034 977 STANFORD RESEARCH INST MENLO PARK CALIF F/G 9/5
MIC 7-TO-11-GHZ FREQUENCY DISCRIMINATOR.(U)
SEP 76 U H GYSEL, J P WATJEN N00039-75-C-0404
UNCLASSIFIED NL

2 OF 2
AD
A034977

END
DATE
FILMED
3-77

coefficients of the sensor and the "source." Both have VSWRs below 1.12:1 over the applicable frequency range. Measurement errors in the two reflection coefficients cause a worst-case efficiency error estimated to be ±0.4%. The efficiency of the sensor is decreased by the losses in the SMA-to-N-type connector adapter at the RF port of the sensor. These losses were measured using the ANA, and the measurement errors were found to lead to an efficiency uncertainty of ±0.25%. Finally, the efficiency of the sensor itself as measured by the manufacturer is known to within ±0.05%. These three types of measurement errors result in a total efficiency error of ±0.7% and a total power measurement error of ±0.72%. This power measurement error and the error associated with the measurement of the discriminator output voltage can be inserted into Eq. (16) to find the resultant error of V'_{vi} or $\Delta V'_{vi}$. The corresponding frequency error Δf_m is obtained from

$$\Delta f_m = \Delta V'_{vi}/\sigma \tag{22}$$

where σ represents the average sensitivity of the discriminator (output voltage change for a given RF frequency change). The power measurement error dominates the total measurement errors and is largest at the edges of the frequency band, as can be seen from Eq. (21). At the bandedges this error is ±16 MHz, and decreases approximately linearly to ±5 MHz at the band center. The dominant error at band center is an assumed uncertainty of ±10 mV in V_{vm} that results from the assumption $V_{vm} = V_{vo}$.

The repeatability of the measurements was excellent, typically much better than ±4 MHz. Thermal-drift problems were minimized because the RF power was applied constantly to the discriminator, except for a few milliseconds that were needed to measure V_{vo}, and because a complete measurement took less than 60 s. A further reduction in the measurement errors is difficult. Moreover, such a step is not justified, because

the ultimate test of the discriminator should be performed in conjunction with a limiter.

In stating the frequency errors of the discriminators, the measurement errors should be included, increasing the worst-case frequency error of our best discriminator (Figure 13) to ±50 MHz. However, the maximum uncertainty of ±16 MHz occurs only at the bandedges. In addition, it is unlikely that the measurement error actually jumps from one limit to the other over a single frequency increment of 100 MHz. If that were the case, the error curve in Figure 13 would be much less smooth. Hence, it is highly probable that the discriminator could be tuned up with a perfect measuring system for a response with a maximum frequency error not exceeding the value obtained under the present imperfect system. Consequently, it is believed that the actual frequency error of the best discriminator is close to the measured value of ±33 MHz.

VII CONCLUSIONS AND RECOMMENDATIONS

Two major goals were achieved in this program. First, a computer program was written that gave the necessary insight into the sources of errors in a line discriminator contributed by subcomponents with practically realizable performances. This computer program was instrumental in determining specifications for the subcomponents of a discriminator designed to achieve a certain maximum frequency error. Second, a microwave-integrated-circuit discriminator was built using microstrip lines on 10-mil-thick sapphire. The frequency error of this discriminator does not exceed ±33 MHz over the full RF range from 7 to 11 GHz at an input power level of -6 dBm, and is at least a factor of four better than that of any known previous discriminator.

Apart from the insight gained from the analysis program, several other factors contributed to the success of the program. Probably the most important factor was the use of a fully integrated microstrip circuit for the entire RF network. This technique elminates numerous interconnections normally present in a circuit with discrete components, and thus removes the origin of deleterious discontinuity VSWRs. In addition, this technique shortens the connecting lines between subcomponents, which results in fewer ripples in the discriminator response. Significant advantages were also obtained from the use of thin-film microstrip circuitry on a sapphire substrate. Higher-performance components can be realized with this technique because circuit patterns are produced with high accuracy.

The dielectric constant of the substrate is stable and predictable, and the components can easily be optimized experimentally. Extensive use

was made of experimental optimization, wherein each subcomponent was tested separately and improved through several iterations. While the MIC approach was essential for obtaining the good performance of the discriminator, it also leads to reduced size, improved reliability, and has the potential for lower cost in production.

It is our belief that a further reduction of the frequency error (±33 MHz) of the present discriminator would be extremely difficult to achieve. The remaining error is due primarily to the residual VSWRs of the two detectors, their remaining unbalance, and the finite isolation of the 3-dB quadrature hybrids. It would be exceedingly difficult to further improve either the detectors or the quadrature hybrids. The periodicity of the ripples observed in the frequency error curve could be reduced by shortening the connecting lines between components on the substrate. However, with the present circuit it is not feasible to reduce the lines to the point where the ripples move out of the band.

The shaping network required to linearize the response adds a degree of complexity to the overall design, even though in a final form it would be integrated on the same substrate as the bulk of the discriminator. A simpler overall system would result if the limiter were designed with an output power that complements the losses of the discriminator. Also, the SNR at the video amplifier output would be improved if the output power level of the limiter were increased. Some improvements in the noise figure of the amplifier itself are possible, but, unfortunately, not to the extent desirable. Finally, the overall size of the discriminator could be reduced substantially with a hybrid integrated video amplifier.

Further development efforts on frequency discriminators should concentrate in three areas. First, improvement in the performance of the discriminator appears possible only with new and different circuits.

While the line discriminator with 3-dB quadrature hybrids is a convenient circuit, the linearity may be improved with other circuits available at lower frequencies by extending the designs to microwave frequencies. Second, a definite improvement in overall accuracy of an open-loop frequency-memory unit could result from development of an integrated package in which the functions of limiter, discriminator, and voltage-controlled oscillator were combined as a single package. In this case, interface problems of impedance level, power level, and so on could be approached from a unified point of view. Moreover, in such a package it would be possible to strive for optimum overall accuracy instead of attempting to force each component to conform to linearity. Finally, there are no fundamental limitations that prevent the present or an alternative design from being extended to higher frequencies. At present, a discriminator design that works at frequencies up to 18 GHz could be realized without major difficulties, and the risk involved in realizing one for even higher frequencies would be modest.

REFERENCES

1. R.J. Mohr, "Broad-Band Microwave Discriminator," IEEE Trans. on Microwave Theory and Techniques, Vol. MTT-11, pp. 263-264 (July 1963).

2. A.Y. Lee, "Signal-Flow Graph-Computer-Aided System Analysis and Sensitivity Calculations," IEEE Trans. on Circuits and Systems, Vol. CAS-21, pp. 209-216 (March 1974).

3. A.F. Podell, "A High Directivity Microstrip Coupler Technique," G-MTT 1970 International Microwave Symposium Digest, pp. 33-36 (May 1970).

4. T. Lange, "Interdigitated Stripline Quadrature Hybrid," IEEE Trans. on Microwave Theory and Techniques, Vol. MTT-17, pp. 1150-1151 (December 1969).

5. B. Schieck, "Hybrid Branchline Couplers--A Useful New Class of Directional Couplers," IEEE Trans. on Microwave Theory and Techniques, Vol. MTT-22, pp. 864-869 (October 1974).

6. A. Uhlir, "Characterization of Crystal Diodes for Low-Level Microwave Detection," The Microwave J., Vol. 5, pp. 59-67 (July 1965).